Towards a ball bouncing demonstration for the T-Flex

S.J. van der Werff

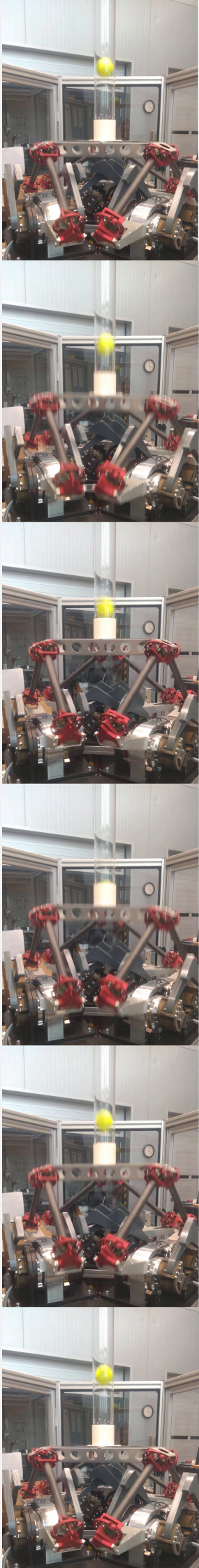

Master's thesis Mechanical Engineering
Chair of Precision Engineering

Examination committee:
prof.dr.ir. D.M. Brouwer PDEng
dr.ir. W.B.J. Hakvoort
ir. B. Seinhorst
dr.ir. A.A. Meghoe

10 February 2023

UNIVERSITY OF TWENTE.

Nomenclature

Subscripts

b	Ball
l	Left
p	Platform
r	Right
x	x-direction
z	z-direction

Superscripts

i	Instance of ball incoming to platform
m	Instance of maximum ball height
o	Instance of ball outgoing of platform

Other symbols

α_b, α_p	Angular acceleration of ball, angular acceleration of platform (rad/s^2)
β	Angle of incidence (rad)
Δp	Linear impulse (kg m/s)
γ	Angle of departure (rad)
ω	Angular velocity of platform (rad/s)
σ	Standard deviation of estimation error of impact time (s)
τ	Actuator torque (N m)
θ	Rotation of platform (rad)
a_b, a_p	Acceleration of ball, acceleration of platform (m/s^2)
d_c	Contact damping (N s/m)
d_s	Support damping (N s/m)
e	Coefficient of restitution

F_d	Damper force (N)
F_s	Spring force (N)
F_t	Tangential contact force (N)
F_c	Normal contact force (N)
$F_{g,b}$, $F_{g,p}$	Gravitational force on ball, gravitational force on platform (N)
g	Gravitational constant (m/s^2)
i	Bounce number
I_b, I_p	Inertia of ball, inertia of platform (kgm^2)
k_c	Contact stiffness (N/m)
k_s	Support stiffness (N/m)
L_p	Length of platform (m)
m_b, m_p	Mass of ball, mass of platform (kg)
M_c	Contact moment (N m)
p	Linear momentum (kg m/s)
r	Distance between location of impact and center of platform (m)
r_b	Radius of ball (m)
t	Time (s)
t_p	Thickness of platform (m)
t_s	Sample time (s)
v_b, v_p	Velocity of ball, velocity of platform (m/s)
x_b, x_p	x-position of ball, x-position of platform (m)
z_b, z_p	z-position of ball, z-position of platform (m)

Summary

Recently, the research chair of Precision Engineering at the University of Twente has developed the T-Flex: a six degree of freedom, fully flexure-based hexapod. It has a translational workspace of 5.5 dm^3, can potentially achieve accelerations up to 18 g, has a repeatability of 0.35 μm RMS and has a high force sensitivity. This combination of properties is unprecedented and therefore the T-Flex is an interesting subject to display the current advancements in flexure-based mechanisms. The goal of this research is therefore to select and develop a suitable demonstration that showcases the combination of these properties.

Based on a literature survey and a set of criteria, a bouncing ball demonstration is deemed most appropriate. An algorithm is developed for vertical, one-dimensional bouncing of a ball on a platform. The objective of this algorithm is to bounce a ball to a given reference height, where the platform velocity at the moment of impact can be regarded as control input to the ball. To calculate the needed platform velocity, the velocity of the ball is relevant. In previously developed ball bouncing algorithms, external sources of information are often used to reconstruct the ball state, such as cameras or force sensors. Due to the high force sensitivity of the T-Flex however, the contact force of the ball on the platform can be obtained from the torque delivered by the actuators and the inverse dynamics model of the T-Flex. The contact force is the basis for measurements as linear impulse and the time between bounces, which are the input to the developed algorithm. The algorithm for one-dimensional bouncing has also been extended to an algorithm for two-dimensional, sideways bouncing.

The one-dimensional bouncing has been verified in a simulation. The two-dimensional bouncing has been simulated as well, as a proof of concept. Additionally, the one-dimensional bouncing has been experimentally tested on the T-Flex. These experiments resulted in two main observations. Firstly, the measurement of linear impulse is 31% lower than expected, the cause of which remains unknown. Secondly, it is found that air resistance is only negligible for bouncing heights lower than 0.25 m. It is therefore recommended that the measurement for the linear impulse is improved and the model for the ball trajectory is extended to account for air resistance, such that higher bouncing is possible. Although the demonstration is not yet completely functional, its feasibility is shown by comparing the required range of motion and acceleration to the properties of the T-Flex.

Contents

1 Introduction **9**

2 Demonstration selection **13**
2.1 Inventarisation of demonstrations 13
2.2 Suitability and ranking 14
2.3 Conclusion 15

3 1D Bouncing **17**
3.1 Outline of the problem 17
3.1.1 Notation 17
3.2 Modelling of the ball impact 18
3.2.1 Coefficient of restitution 18
3.2.2 Model of the mechanism 19
3.3 Overview of the control scheme 20
3.4 Obtaining measurements 20
3.5 Estimation problem: ball trajectory prediction 21
3.5.1 Backward estimation 22
3.5.2 Forward estimation 22
3.5.3 Estimation of first bounce 23
3.6 Control problem: height regulation 23
3.7 Platform trajectory generation 24
3.8 Simulations 26
3.8.1 Simscape model 26
3.8.2 Results 27

4 2D Bouncing **33**
4.1 Outline of the problem 33
4.1.1 Notation 33
4.2 Modelling of the ball impact 34
4.3 Overview of the control scheme 35
4.4 Obtaining measurements 35
4.5 Estimation problem: ball trajectory prediction 36
4.5.1 Backward estimation 36
4.5.2 Forward estimation 36
4.5.3 Estimation of first bounce 37
4.6 Control problem: height and distance regulation 38
4.7 Platform trajectory generation 39
4.8 Simulations 40
4.8.1 Simscape model 40

4.8.2 Results . . . 41

5 Emperical results and feasibility **45**
5.1 The T-Flex . . . 45
5.2 Estimation of the contact force . . . 45
5.3 Estimation of the impact location . . . 47
5.4 Development of a new ball trajectory formulation . . . 47
5.4.1 Motivation for the alternative formulation . . . 48
5.4.2 Derivation of analytical relations . . . 49
5.4.3 Conclusion . . . 51
5.5 Emperical results . . . 51
5.5.1 Set-up . . . 51
5.5.2 Method . . . 51
5.5.3 Tests without moving platform . . . 52
5.5.4 Tests with moving platform . . . 55
5.6 Feasibility . . . 59
5.6.1 Allowed workspace . . . 59
5.6.2 Required time for the trajectory . . . 60
5.6.3 Extension to longer constant velocity . . . 60
5.6.4 Higher bouncing height . . . 61
5.6.5 Conclusion . . . 61

6 Conclusion **63**

7 Recommendations **65**

A Rubric for scoring criteria of demonstration choice **71**

B Calculation of platform trajectory 1D bouncing **73**

C Simulation model 1D bouncing **77**

D Derivation of the angle of departure **79**

E Derivation of the reference angle for the platform **81**

F Calculation of platform trajectory 2D bouncing **83**

G Simulation model 2D bouncing **85**

H Plagiarism Report **87**

Chapter 1

Introduction

Recently, the research chair Precision Engineering at the University of Twente has developed the T-Flex: a six degree of freedom (DOF), fully flexure-based hexapod [1]. A photograph is shown in Figure 1.1. The design of the T-Flex aims to combine the advantages of parallel kinematic manipulators (PKMs) with the advantages of flexure joints. PKMs are interesting for high-precision tasks because they allow for high accelerations, due to low moving mass, and higher repeatability because of their higher rigidity [2]. Using the joints shown in [3], [4], the range of motion of a flexure-based PKM can be increased, while play and friction are still avoided. The T-Flex is able to travel a workspace of 5.5 dm^3 and achieves a repeatability of 0.35 μm RMS. Accelerations of up to 18 g can potentially be achieved. Moreover, the torque feedback has a resolution of 6 Nmm, which, in combination with the backdrivability due to the absence of friction, results in a high force sensitivity. The resulting resolution of the measured force on the end-effector is 0.00314 N in neutral position. This combination of properties is unprecedented and therefore it is an interesting subject to display the current advancements in flexure-based mechanisms.

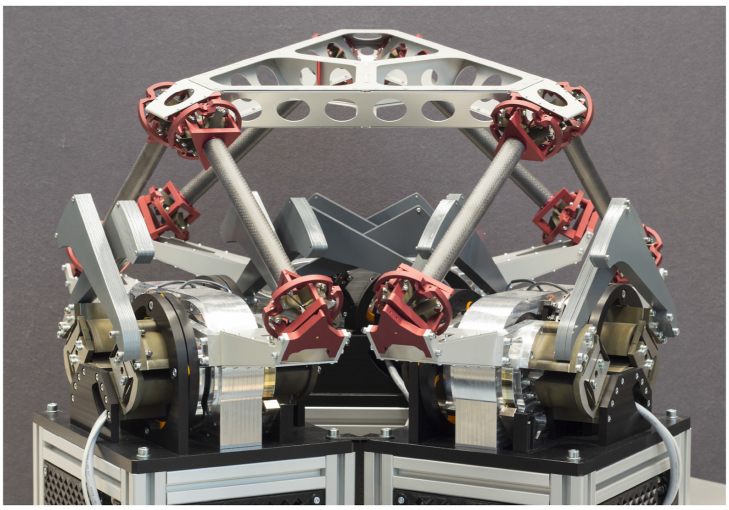

Figure 1.1: The T-Flex [1].

To demonstrate the workspace and motion of the T-Flex, several pre-programmed trajectories are already available. These include a sequence of translations and rotations, a swirl that combines translation and rotation, and variations on both, some of which are shown in [5]. However, there is not yet a demonstration of the mechanism that displays the repeatability and force sensitivity in combination with the acceleration and stroke. Such a demonstration is desired, to show these

capabilities and in particular the combination of them.

The first goal of this research is to select a suitable demonstration to show the capabilities of the T-Flex. Examples of existing demonstrations are executing a pre-planned movement [6]–[8], a pick and place task [9], [10], balancing or bouncing an object [11]–[13] or an optical demonstration [14]–[16]. In Chapter 2, an inventarisation has been made of existing demonstrations and a suitable demonstration is selected. A bouncing ball demonstration is found to be most appropriate to showcase the capabilities of the T-Flex.

The second objective of this research is to develop and validate this demonstration. There are multiple examples of bouncing, also called batting, manipulators. Examples of batting actions are playing table tennis or baseball. A series of consecutive, periodic batting motions is often referred to as juggling. With juggling, the ball has a free flight through the air, whereas during dribbling, the ball undergoes contact with a surface in the midst of its free-flight phase [17]. All of these motions have in common that reliable information on the ball state is essential to hit and aim the ball correctly. From literature, several methods of gathering this information can be found.

The first method is using cameras or motion capture systems. With this information, the ball trajectory can be predicted [18]–[21]. Alternatively, the ball can be tracked on the camera footage, while the paddle makes an opposite and scaled-down motion compared to the ball [12], [22]. This is an adoption of the so-called mirror algorithm [23], where the robot reference trajectory is a function of the ball position. Secondly, methods that require no information on the ball state at all have been developed as well. Those employ a periodic motion of the bouncing surface, resulting in stable bouncing of the ball [24]. This periodic motion can be combined with a concave paddle to stabilise the horizontal motion of the ball [13], or the periodic motion can be implemented on two separate arms, resulting in two-dimensional juggling [25]. Next to this, there are methods that gather information on the ball state only when the ball is in contact with the end-effector. This information is used in models of the ball rebound and flight. A control scheme for vertical bouncing that only takes impact times and table motion as input has been proposed [26], as well as a scheme that includes an impact predictor based on impact times and a collision detector based on the equations of motion of the end-effector [27]. A cooperative juggling set-up, using two delta robots that face each other and bounce a ball back and forth, uses multiple force sensors mounted on the end-effectors [28]. These are used for the estimation of the impact location and impact times. In [29], a comparison has been done on basketball dribbling with input from a vision system and force and torque sensors that are mounted on the end-effector. In the case of the force and torque sensor, the ball trajectory is constructed using projectile motion equations, the conservation of momentum and the coefficient of restitution. The force and torque based approach appears to be less successful than the vision based approach because the estimates for the coefficient of restitution are not precise enough, the force and torque measurements contain a lot of noise due to the moving end-effector and the assumption is done that the ball does not move horizontally during dribbling, while it in fact does travel horizontally in the experiments. Lastly, a variation on estimating the ball trajectory and rebound properties only during impact without visual systems is done by using accelerometers on rackets. This is shown for both tennis rackets [30] and table tennis paddles [31].

There are multiple bouncing demonstrators that show that a correct estimation of the ball trajectory can be obtained without cameras or motion capture systems. However, to achieve closed-loop bouncing, these demonstrators do require additional sensors, such as a force sensor

or accelerometer. The use of additional sensors might introduce limitations, for example, additional noise when mounted on the end-effector [29], limited measurements in certain directions, such as tangential forces, drift, or additional costs and complexity. These limitations can be reduced by employing the high force sensitivity of the T-Flex, to gather information on the ball state during collision. The contribution of this research is therefore the development of an active bouncing algorithm that utilises solely the feedback from the encoders and actuators of the T-Flex. This information is used to reconstruct and predict the ball trajectory. Due to the force-sensitivity of the T-Flex, the forces and torques exerted on the end-effector, due to the impact, can be measured. From this, the change in velocity and the impact location can be calculated, regardless of where this is on the end-effector. This poses the opportunity for unconstrained one-dimensional and two-dimensional bouncing. With the predicted ball trajectory, the platform velocity, which is the control input to the ball, can be calculated and the ball can be bounced towards a given reference height.

The remainder of the report is structured as follows. In Chapter 2, the selection of a suitable demonstration is discussed. A theoretical framework of one-dimensional ball juggling and the validation thereof by simulation is presented in Chapter 3. This will be extended to two-dimensional juggling in Chapter 4. Empirical validation of the one-dimensional bouncing is described in Chapter 5. In Chapter 6, conclusions are drawn and recommendations for future work are given in Chapter 7.

Chapter 2

Demonstration selection

The T-Flex is a 6DOF, fully flexure-based hexapod, that is able to achieve high accelerations, high repeatability, high force sensitivity and a large workspace. The combination of these properties poses an interesting case to show the advancements in flexure-based mechanisms. For this reason, the T-Flex will be displayed at events such as fairs. This requires that the demonstration should be both appealing to the public and an effective way of showing its features. To this end, a suitable type of demonstration needs to be determined. By finding examples of demonstrations and classifying those demonstrations into several categories, an inventory can be made of what features of the T-Flex each category could highlight. Each category will be scored on its suitability by using a set of criteria that the demonstration should satisfy. A demonstration will be selected based on this ranking.

2.1 Inventarisation of demonstrations

There are many examples of demonstrations for different kinds of robots and manipulators. For this research, the focus is mainly on robots with parallel kinematics, such as hexapods, Stewart platforms, delta robots, as the T-Flex is a PKM as well. Demonstrations that can be found are for example exhibitions of a setup on a fair. Furthermore, inspiration can also be found in the applications of industrial robots, the showcasing of a final project of a study programme, or demonstrating a self-built robot. In addition, research on control theory and dynamic systems might also result in experiments that have demonstrative value and are therefore interesting as well.

The found demonstrations can be divided into several categories:

- **Pre-planned movements**: The robot follows a set of prescribed movements, demonstrating its range, velocity and accelerations, for example. This can be extended with an additional element, such as drawing a figure [32], moving through a grid of obstacles [6] or milling a pyramid [8], shown in Figure 2.1.
- **Pick and place**: A gripper picks objects and places them somewhere else. Either the gripper is static and the platform moves, or vice versa. Examples are the Micro Gripper of SmarAct [9] that is used for microassembling, shown in Figure 2.2, or a delta robot demonstrating its velocity by moving around golf balls [33].
- **Balancing an object**: The manipulator balances an object, for example, a ball. When the object is pushed away from its resting point or trajectory, this will be corrected. In the case of balancing a ball, the sensing of the ball position can be done with a touchpad

[11] or a camera [34]. Another example is the upswing and balancing of a triple pendulum on a 1DOF stage [35], see Figure 2.3.

- **Throwing and/or catching an object:** The robot throws an object and might catch it again or throw it in an area somewhere else. In addition, there are also robots catching objects based on camera input. An example of a robot throwing objects, regardless of their shape and weight, is the TossingBot [36]. Examples of catching robots are a 6DOF, cable-driven basketball hoop [37], or a catching hand [38]. Examples of juggling robots, that throw and catch continuously, are Cassie Cal [12] which uses a camera to track the ball and the Blind Juggler and its derivatives [13], [39], [40] that stabilise the bouncing by a concave bowl and consistent periodic motion. Cooperative juggling between two delta robots, using only force sensors, has been explored as well [28]. An image of a simulated juggling session from this is shown in Figure 2.4. Another example is juggling with a triple pendulum between two quadcopters, using the input of a motion capture system [41].

- **Optical**: The manipulator uses for example lights, lasers and visual patterns to show its performance or accuracy. The SmarAct interferometer shows when a sensor head is aligned, by aligning two light spots [15]. PI shows fibre alignment by letting light run through the fibre as soon as it is aligned [14], Figure 2.5. Lastly, the repeatability of a 6DOF platform can be shown by using for example laser crosses [16].

- **Motion simulation**: Flight and race car simulations are examples of motion simulations. A person is seated on top of the platform and experiences the motion of the vehicle in 6DOF, such as demonstrated with a motorcycle simulator [42], shown in Figure 2.6, or an airplane simulator [43].

2.2 Suitability and ranking

The demonstrations are evaluated for their suitability. First, it is investigated which of the four capabilities of the T-Flex are shown for each demonstration category. Then, the categories are evaluated on the amount of needed additional hardware, the amount of preparation that will be needed, the supervision needed during the demonstration, the ability to adjust or extend the demonstration, and the originality and attractiveness of it.

Since the T-Flex has a simultaneous travel range of ± 50 mm in x, y and z direction and can carry a maximum vertical payload of up to twenty kilograms [1], the motion simulation demonstration is deemed not feasible. Therefore, this category is omitted. The other categories and their scoring is shown in Table 2.1. The first four criteria are the capabilities of interest: can a demonstration show the possible acceleration, workspace, repeatability and current sensitivity of the T-Flex? This is ranked with a yes or no. For the other categories, the scoring is done on a scale of one to five, where a lower score indicates a less beneficial situation. The exact rubric is included in Appendix A. For the needed hardware, it is taken into account whether the demonstration requires additional objects and the effort it takes to install or mount these. The amount of preperation that is needed to get the demonstration working is evaluated, as well as the amount of needed supervision. A demonstration that requires continuous supervision or regular intervention scores lower. The ability to adjust or extend the demonstration is evaluated as well. Lastly, an indication is given of how well the demonstration would stand out at a fair or event, based on its originality and how captivating it could be. The given scores are summed and result in a total score, indicating the suitability of the demonstration.

Table 2.1: The scoring of the potential categories for the demonstration. The categories are scored on a scale of 1 to 5, where 1 indicates that the category scores worst, and 5 is best.

	Pre-planned movement	Pick and place task	Balancing an object	Optical	Throw and/or catch
Acceleration	✓	✓	✓	✓	✓
Workspace	✓	✓		✓	✓
Sensitivity			✓		✓
Repeatability	✓	✓		✓	
Additional hardware	5	1	4	2	4
Preparation	5	2	4	3	4
Supervision	5	4	3	4	1
Adjust/extend	3	3	2	4	5
Originality and attractiveness	2	3	3	4	5
Total	21	16	21	20	22

2.3 Conclusion

From the ranking, it appears that throwing and catching scores highest overall, although differences are small. The pre-planned movement demonstration scores lowest on attractiveness and such a demonstration is already implemented on the T-Flex. The pick-and-place appears to be the most complex demo. For these reasons, the pre-planned movement and pick-and-place demonstrations will not be considered. None of the demonstrations is able to show all four capabilities, so a combination of demonstrations is to be considered. To achieve a demonstration that shows three out of four capabilities, the throwing and catching and the balancing of an object will be combined by juggling a ball. Through this, a demonstration can be achieved that requires little additional hardware and preparation, is attractive and original, but requires less supervision than just throwing or catching. However, this type of demonstration means that the repeatability will not be shown. Therefore, the juggling could be combined with an optical element as well, for example a laser pointing to fixed locations, to also show the repeatability of the T-Flex.

Figure 2.1: Milling of a pyramid using a pre-planned path, video still adapted from [8].

Figure 2.2: Pick-and-place demonstration by [44].

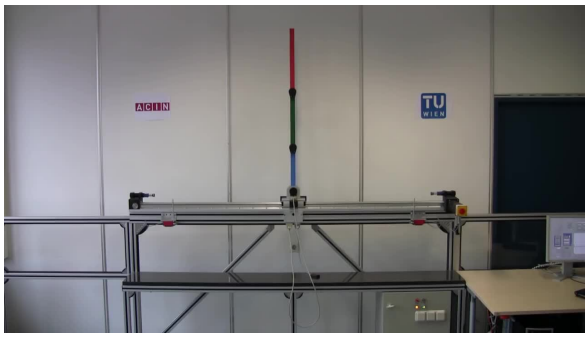

Figure 2.3: Balancing demonstration using a triple pendulum on a 1DOF cart, video still adapted from [45].

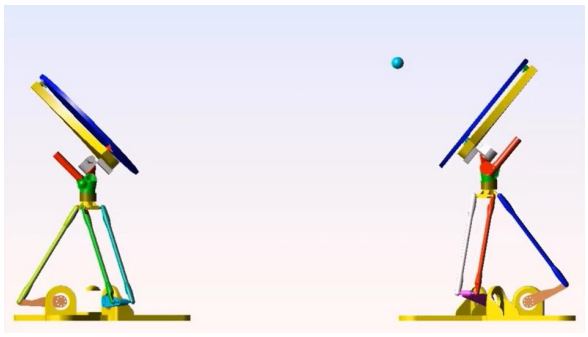

Figure 2.4: Simulation of a cooperative juggling demonstration, video still adapted from [46].

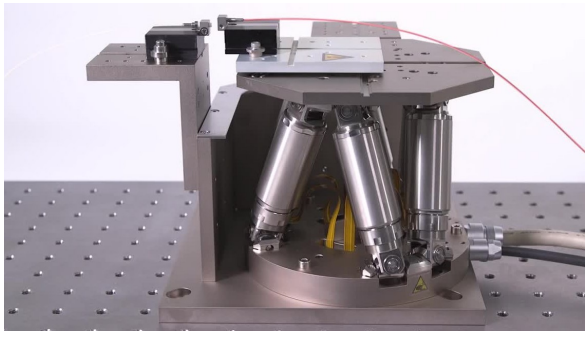

Figure 2.5: Optical fibre alignment demonstration, video still adapted from [14].

Figure 2.6: Motorcycle motion simulator, video still adapted from [42].

Chapter 3

1D Bouncing

3.1 Outline of the problem

The T-Flex is a fully flexure-based hexapod, resulting in no mechanical damping or hysteresis in any of the joints and the actuator suspension. For this reason, no energy is dissipated in these joints during motion. This implies that the force that is exerted onto the end-effector can be reconstructed using kinematic and dynamic relations and the torque feedback of the actuators and the measurements of the encoders. This provides the opportunity to model interactions between the end-effector and external objects. The goal is to achieve active bouncing of a tennis ball using solely the information that can be obtained during the collision. The bouncing will be one-dimensional, so only straight up and down, see Figure 3.1 for an illustration of the vertical bouncing on the T-Flex.

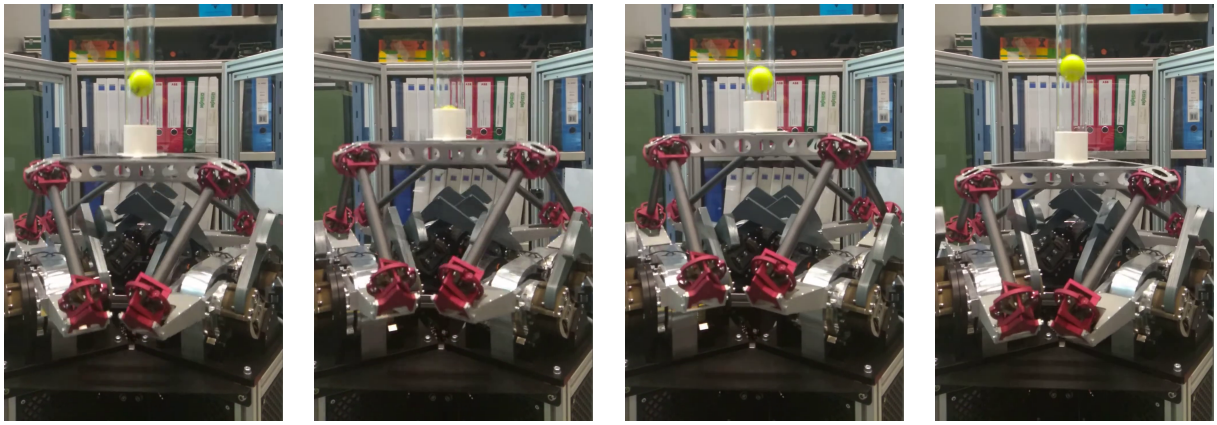

(a) Ball falls down, end-effector moves upwards.

(b) Impact.

(c) Ball goes up, end-effector reaches highest position.

(d) Ball reaches highest position, end-effector is moving downward.

Figure 3.1: One-dimensional bouncing on the T-Flex. A tube is mounted on the end-effector, to constrain the ball to a vertical movement.

3.1.1 Notation

To establish a clear notation, each bounce is divided into three instances, which are visualised in Figure 3.2. One single bounce is indicated with the index i. The consecutive bounce will be referred to as bounce $i + 1$. The start of the bounce is defined as the moment when the ball

leaves the platform. The end of the bounce is right before the ball leaves the platform again for the next bounce. This means that the flight time, consecutive impact and related measurements are all indicated with index i. During each bounce, three main events can be distinguished. The first is leaving the surface, denoted by the superscript o, for *outgoing*. The moment of reaching maximum bouncing height is indicated with m, for *maximum*. Lastly, the moment right before impact is denoted by i, for *incoming*. Additionally, all properties related to the ball will be indicated with subscript b and similarly for the platform with subscript p. Height $z_b^o[i]$, for example, refers to the height of the ball at the moment of leaving the surface during bounce i. In the one-dimensional scenario, all positions, velocities and accelerations are in z-direction.

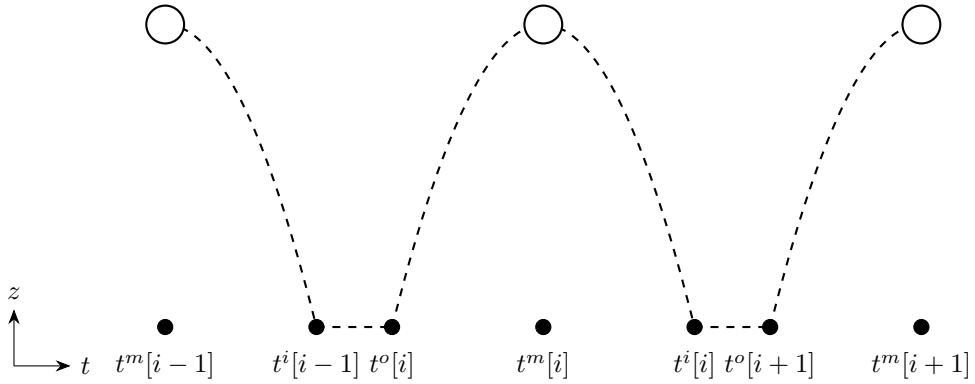

Figure 3.2: A bouncing trajectory of a ball over time. The ball leaves the surface at time $t^o[i]$, it reaches the maximum height of the parabola at time $t^m[i]$ and hits the surface again at time $t^i[i]$. Between $t^i[i]$ and $t^o[i+1]$, the ball is in contact with the surface.

3.2 Modelling of the ball impact

In this section, the collision between the ball and the platform is modelled. First, an explanation of the coefficient of restitution is given. Next, the dynamics of the ball and platform are analysed and several assumptions for the impact and ball flight are presented.

3.2.1 Coefficient of restitution

During a collision between the ball and surface, energy will be dissipated, resulting in a loss in kinetic energy of the ball. Such collisions are known as inelastic collisions. On the other hand, an elastic collision is an idealised collision, where no energy loss takes place. The loss of kinetic energy can be described by the coefficient of restitution (COR), denoted by e, which has a value between 0 and 1. A COR of 0 denotes a fully inelastic collision, where a total loss of energy takes place and as a result, the ball sticks to the surface. A COR of 1 describes an entirely elastic collision, without energy loss. When only translational velocities are taken into account, the COR can be expressed as

$$e = \frac{v_b^o[i] - v_p^o[i]}{v_p^i[i-1] - v_b^i[i-1]}, \tag{3.1}$$

where v_b and v_p are the velocity of the ball and the platform in $z-$direction [47]. Factors that heavily influence the COR are the type of ball and the surface [48]. However, for any given combination of these two, the COR will vary from bounce to bounce as well, as it is influenced by, among others, the ball velocity and incident angle [49]. To simplify the analysis, the COR

is assumed to be constant. During the tests, a standard, pressureless tennis ball will be used, indicated as a type 2 ball by the International Tennis Federation. This type of tennis ball has a COR between 0.728 and 0.762 in standardised tests [50]. These tests are done on a smooth and rigid horizontal surface, although no material is specified. From here on, the COR of a tennis ball is assumed to have a constant value of 0.75, which shows to be an appropriate value from the tests (Section 5.5).

3.2.2 Model of the mechanism

The T-Flex consists of an end-effector, supported by 3 pairs of arms and actuators. Additionally, a PID controller is imposed on the mechanism, which introduces stiffness and damping as well. A simplified, 1DOF model is constructed for analysis. All mass has been lumped into a mass that resembles the end-effector. The individual stiffnesses are gathered into a lumped stiffness represented by a spring and similarly for the damping, represented by a damper. This model forms the basis for the simulations as discussed in Section 3.8.

In this model, the platform and ball both only move in z-direction. It is assumed that the platform does not rotate and the ball does not spin. Therefore, all effects due to ball spin are neglected. Air resistance is neglected as well. Additionally, the ball is assumed to impact at the center of the platform.

A free body diagram of the modelled mechanism, together with the ball, is shown in Figure 3.3. Before impact, only the gravitational force $F_{g,b}$ is acting on the ball. The end-effector also has a gravitational force, $F_{g,p}$, as well as the modelled spring and damper force, F_s and F_d. The platform is initially at rest. During impact, a contact force F_c exists, which is acting on both the platform and the ball. The contact force on the ball is equal in magnitude but in opposite direction of the contact force on the platform. The equation of motion for the ball is

$$m_b a_b = F_c - F_{g,b}, \tag{3.2}$$

where m_b is the mass of the platform and a_b is the acceleration of the platform.

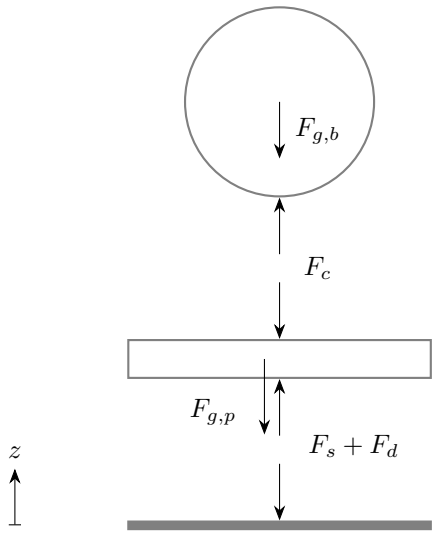

Figure 3.3: Free body diagram of the ball and a 1DOF platform. The platform is supported by a spring and damper. Both the ball and the platform only move in z-direction.

3.3 Overview of the control scheme

In Figure 3.4, an overview is shown of the control scheme for the bounce height. Given the measurements for linear impulse Δp and time between bounces Δt, we would like to calculate the platform velocity v_p, to bounce the ball to a given reference height z_{ref}.

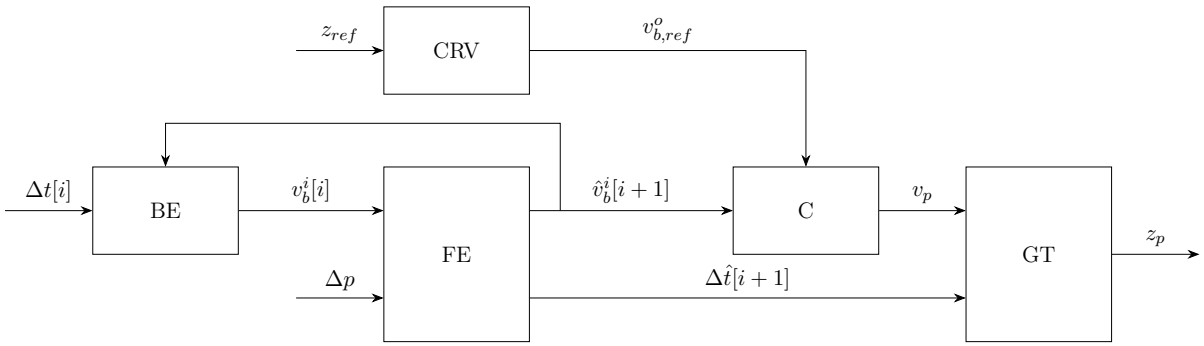

Figure 3.4: Block diagram for the control problem of bouncing a ball to a given reference height.

Immediately after the impact starts, the measurement $\Delta t[i]$ is available. This is the input for the backward estimation (BE), which outputs the incoming velocity of the ball $v^i_b[i]$. After the impact has finished, $\Delta p[i]$ is available as well. Both $v^i_b[i]$ and $\Delta p[i]$ are input for the forward estimation (FE), which predicts the incoming ball velocity $\hat{v}^i_b[i+1]$ and time of impact $\Delta\hat{t}[i+1]$ for the next bounce. The hat indicates a predicted value.

A reference bounce height z_{ref} is given, from which a reference ball velocity $v^o_{b,ref}$ can be calculated, represented by the block calculate reference velocity (CRV). $v^o_{b,ref}$ and $\hat{v}^i_b[i+1]$ are input for the controller (C), which calculates the necessary platform velocity v_p during the following bounce. Both v_p and $\Delta\hat{t}[i+1]$ are then used to generate a trajectory (GT) for the end-effector, resulting in a reference position profile z_p for the end-effector.

In the following sections, the measurements $\Delta t[i]$ and $\Delta p[i]$ will be specified and the calculations for each block will be derived.

3.4 Obtaining measurements

The only moment of obtaining information about the ball state is during collision, which results in the measurements that serve as input for the parameter estimation. This section is about how these are obtained, as well as finding the position of the ball during impact.

The contact between the ball and the platform introduces a contact force, F_c, as explained previously in Section 3.2.2. In simulations, the contact force acting on the ball can directly be obtained from a Simscape function modelling the contact, which is discussed in Section 3.8.1. On the T-Flex, the contact force acting on the platform can be obtained by comparing the expected actuator torques, from the inverse dynamics model, with the actual actuator torques. This is elaborated in Section 5.2.

The contact force is directly related to the change in linear momentum p of the ball and plat-

form, which, in turn, is directly related to the change in velocity of both. This change in linear momentum is called the linear impulse Δp, defined as

$$\Delta p[i] = \int_{t^i[i]}^{t^o[i+1]} m_b a_b \, dt = \int_{t^i[i]}^{t^o[i+1]} F_c - F_{g,b} \, dt, \tag{3.3}$$

where t^i and t^o indicate the time of the start and end of the collision, respectively, and $m_b a_b$ follows from Equation (3.2).

Another relevant measurement in describing the ball trajectory is the time between two consecutive bounces, denoted by Δt. The time between two bounces is described as

$$\Delta t[i] = t^i[i] - t^o[i]. \tag{3.4}$$

The definition of the start and end of a bounce differ for the simulation and the empirical verification. This will be discussed in Section 3.8 for the simulations and in Section 5.5 for the experiments.

The position of the ball is defined as the position of the center of the ball. The ball state will be expressed in the global frame, which is located at the ground, see Figure 3.3. The platform position, velocity and acceleration are fully known, because of the kinematic relations between the actuators and end-effector, as described in [51]. The ball position is therefore also known at the start and end of the impact, as this can be expressed as

$$z_b^i[i] = z_p^i[i] + r_b \tag{3.5}$$

and

$$z_b^o[i] = z_p^o[i] + r_b. \tag{3.6}$$

Here, z_b is the z-position of the ball, z_p is the z-position of the platform and r_b is the radius of the ball.

3.5 Estimation problem: ball trajectory prediction

In order to do active bouncing, it is necessary to first obtain a formulation for the ball trajectory. To this end, the ball trajectory is parameterised by the ball velocity. From the ball velocity, is possible to obtain expressions for the ball height and the time between two bounces. The purpose of this velocity estimation is to obtain an expression for the ball velocities without using the COR, as the exact value of it is unknown and varies for each bounce. Therefore, the measurements as described in Section 3.4 are used, in combination with physics-based relations.

The estimation problem can be divided into two separate estimations: the backward estimation and the forward estimation. The backward estimation occurs right after the initial contact between the ball and the platform, as it takes the measurement $\Delta t[i]$ as input. The forward estimation is done after the collision is fully completed, so the measurement $\Delta p[i]$ is available, and when the backward estimation is done, such that $v_b^i[i]$ is available. See Figure 3.5 for a schematic representation. Both estimations are explained in this section, as well as how they can be adjusted for the first bounce after dropping the ball.

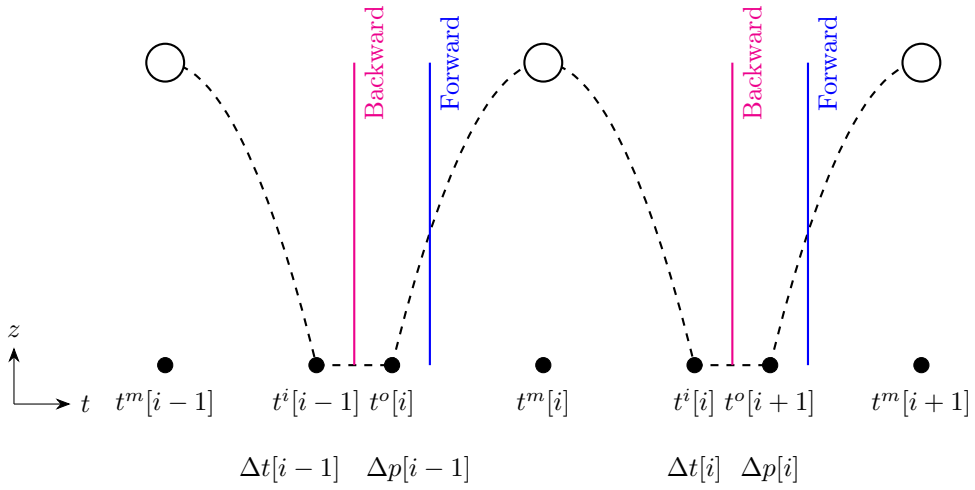

Figure 3.5: One-dimensional bouncing ball trajectory over time, with the approximate moments of the backward estimations (magenta) and the forward estimations (blue). The available measurements are indicated below the timestamps.

3.5.1 Backward estimation

At the moment of the backward estimation between bounce i and bounce $i+1$, the available measurement is the time between the current and previous bounce, $\Delta t[i]$. Additionally, from the previous forward estimation, the prediction for the incoming ball velocity $\hat{v}_b^i[i]$ is known. The desired output is $v_b^i[i]$, the calculated incoming ball velocity.

The incoming velocity of the ball can be calculated using the measurement $\Delta t[i]$ and the position of the ball on the platform. From the expression of the position of the ball

$$z_b^i[i] = z_b^o[i] - v_b^i[i]\Delta t[i] - \frac{1}{2}g(\Delta t[i])^2, \tag{3.7}$$

we can solve for $v_b^i[i]$, which gives

$$v_b^i[i] = \frac{(z_b^o[i] - z_b^i[i])}{\Delta t[i]} - \frac{1}{2}g\Delta t[i]. \tag{3.8}$$

This calculated value of the ball velocity is used to correct the prediction of the ball velocity, by taking the average of the input $\hat{v}_b^i[i]$ and the calculated value $v_b^i[i]$.

3.5.2 Forward estimation

At the moment of the consecutive forward estimation, the available measurement is the linear impulse $\Delta p[i]$. The other input is the incoming ball velocity $v_b^i[i]$ from the backward estimation. Parameters that can now be estimated are the predicted incoming ball velocity for the next bounce, $\hat{v}_b^i[i+1]$, and the prediction for the moment of the next bounce, $\Delta\hat{t}[i+1]$.

The outgoing ball velocity is used in the calculation of $\Delta\hat{t}[i+1]$. Using the conservation of momentum, the outgoing ball velocity can be related to the incoming ball velocity as

$$v_b^o[i+1] = v_b^i[i] + \frac{\Delta p[i]}{m_b}. \tag{3.9}$$

The estimation of $\Delta\hat{t}[i+1]$ is based on the nominal bouncing situation: the ball hits the platform when it is in its neutral position, which is the reference position for the platform when no movement is required. The height of the ball at time $t^i[i+1]$ can be expressed as

$$z_b^i[i+1] = z_b^o[i+1] + v_b^o[i+1]\Delta\hat{t}[i+1] - \frac{1}{2}g(\Delta\hat{t}[i+1])^2. \tag{3.10}$$

This polynomial can be solved for $\Delta\hat{t}[i+1]$, resulting in

$$\Delta\hat{t}[i+1] = \frac{v_b^o[i+1]}{g} + \sqrt{\left(\frac{v_b^o[i+1]}{g}\right)^2 + \frac{2}{g}(z_b^i[i+1] - z_b^o[i+1])}. \tag{3.11}$$

Since the velocity is in vertical direction and therefore subject to gravitational acceleration, the estimate for the incoming velocity is

$$\hat{v}_b^i[i+1] = v_b^o[i+1] - g\Delta\hat{t}[i+1]. \tag{3.12}$$

3.5.3 Estimation of first bounce

The start of a bouncing sequence is schematically visualised in Figure 3.6. At the start of the bouncing sequence, the ball is released from a known height z_{drop}. The value for z_{drop} is set by the user of the demonstration. $\Delta t[1]$ can therefore not be measured, as the time of release is unknown. The estimate of the incoming velocity $\hat{v}_b^i[1]$ is not available either, since there is no preceding forward estimation. Information that is available however, is the measurement of $\Delta p[1]$ during the first collision. For these reasons, the first backward estimation is adjusted.

Since the height from which the ball is released, z_{drop}, is known, the incoming ball velocity can be found by

$$v_b^i[1] = -\sqrt{2g(z_{drop} - z_b^i[1])}. \tag{3.13}$$

After this, all forward and backward estimations can take place as described earlier.

3.6 Control problem: height regulation

With the estimated velocities and impact time from the forward and backward estimation, the required control input for the ball can be calculated. This control input is the platform velocity. An expression for this will be derived in this section.

For the height regulation of the ball, a reference bounce height z_{ref} is given. From this, a reference velocity for the ball can be calculated: the velocity that the ball should have when leaving the platform, to obtain this height. From the conservation of energy, a function for CRV (see Figure 3.4) can be found:

$$v_{ref} = \sqrt{2g(z_{ref} - z_b^o)}. \tag{3.14}$$

To be coherent with to the calculation of $\Delta t[i+1]$ in Equation (3.11), z_b^o is chosen to be the neutral position of the platform.

This reference velocity v_{ref} is input to the controller C, as is the predicted incoming velocity of the ball $\hat{v}_b^i[i+1]$. From both, the height regulation of the ball can be constructed. The

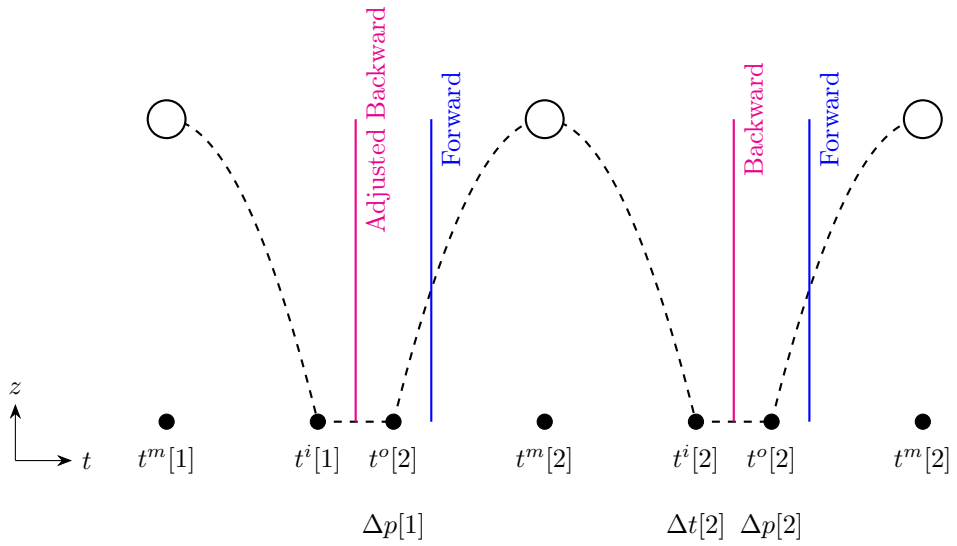

Figure 3.6: Beginning of the bouncing ball trajectory, plotted over time, with the moments of the first backward estimations (magenta) and the forward estimations (blue). The available measurements are shown below the timestamps. At time $t^m[1]$, the ball is dropped from an arbitrary, but known height z_{drop}.

outgoing ball velocity is related to the incoming ball velocity and the platform velocity by the COR, as shown in Equation (3.1), where it is assumed that the platform velocity is unaffected during the impact ($v_p = v_p^i[i+1] = v_p^o[i+2]$). This assumption is motivated by the conservation of momentum, since the mass of the platform is approximately a factor 16 larger than the mass of the ball. This is calculated with a tennis ball with $m_b = 0.057$ kg and the T-Flex with an end-effector of $m_p = 0.91$ kg. The reference platform velocity can be calculated as

$$v_p = \frac{v_b^o[i+2] + e v_b^i[i+1]}{1+e}. \tag{3.15}$$

3.7 Platform trajectory generation

In this section, a position profile for the end-effector is obtained, using the estimated impact time from the forward estimation and the platform velocity from the controller.

The desired trajectory for the end-effector consists of a linear part, with constant velocity v_p, and polynomials of second and third order. In Figure 3.7, a generalised trajectory is shown, with the position in z-direction plotted against the time.

The ball is predicted to impact the end-effector at time t^i and the height of the platform at t_i is chosen to be the neutral position. At the time of impact, the platform should have the velocity v_p as calculated in Equation (3.15), to make sure that the ball bounces to the reference height. To account for prediction errors in t^i, there is an interval over which the platform moves with constant velocity. This interval has a width of 2σ, where σ is the standard deviation of the prediction error for t^i. See Section 5.5 for an elaborated explanation. Using a constant velocity interval with a duration of 2σ, approximately 68% of all bounces can be correctly intercepted.

The calculation of the platform motion profile is discussed in Appendix B. After the genera-

tion of the motion profile, it can be verified whether it is within the range of the T-Flex, whether the trajectory is feasible in the available time and if the acceleration of the entire profile is indeed below the limits, because of the third order polynomial for the position. For the case where the ball height in the previous bounce, $z_b^m[i-1]$ was 0.2 m, the reference bounce height, z_{ref}, is 0.2m, the COR is 0.75 and σ is 0.5 s, the position velocity and acceleration profiles are shown in Figure 3.8. The impact time is at 0.6 s.

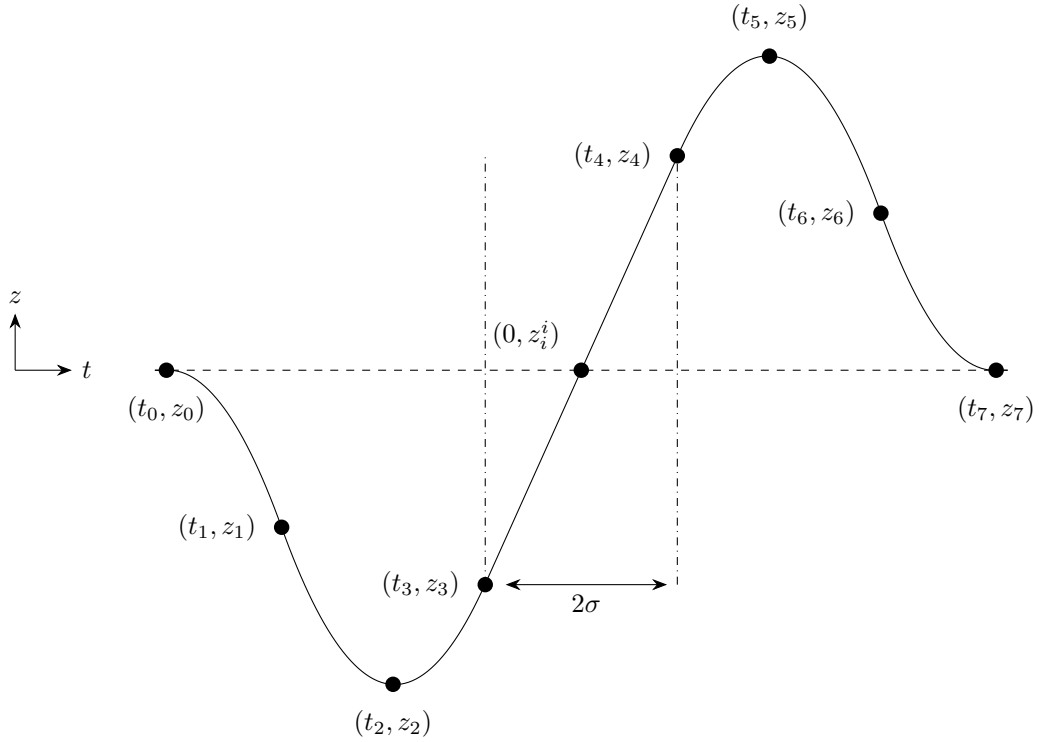

Figure 3.7: Generalised image of the platform trajectory in z-direction over time, to do one-dimensional bouncing. The expected impact time of the ball on the platform is t_i^i. The platform has a constant velocity for a duration of 2σ, between t_3 and t_4. Here, σ is the estimation error of t_i^i.

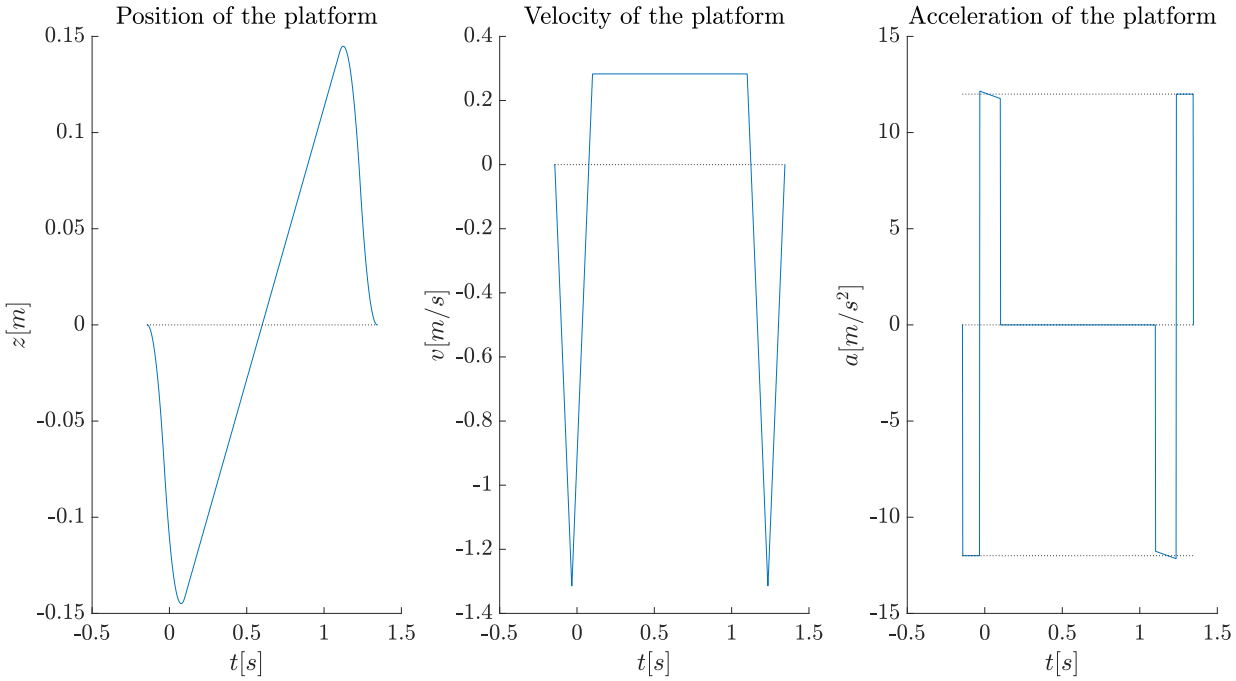

Figure 3.8: Profiles for the position, velocity and acceleration, in the situation where $z_{ref} = 0.2$ *m,* $z_b^m[i-1] = 0.2$ *m,* $\sigma = 0.5$ *s and* $e = 0.75$*. The estimated impact time is at* 0.6 *s.*

3.8 Simulations

The theoretical framework that is established in the previous sections has been verified with simulations. First, an overview of the used simulation model and settings is given. Next, the results from the simulations are presented and discussed.

3.8.1 Simscape model

The used software is Matlab 2018a with Simscape. To model the contact between the ball and the platform, the Simscape Multibody Contact Force Library [52] has been used. An image of the used model is shown in Appendix C. The sample time t_s of the simulation is 0.001 s.

The model as presented in Figure 3.3 is the basis for this simulation. The supporting spring and damper are a simplified, mechanical representation of T-Flex itself and the controller. The ball is modelled as a spherical solid with a radius r_b and mass m_b of a standard tennis ball. It has three DOFs (x, z and θ) with respect to the ground, which is modelled as a plate rigidly attached to the global frame. Above the ground are two other plates, both rectangular shaped and with the same mass m_p, length L_p, thickness t_p and width w_p. The lower of these plates, called middle plate, can only translate vertically with respect to the ground and is actuated by a prescribed motion profile. The platform is placed above the middle plate. The middle plate and platform can translate vertically and rotate with respect to each other. This is not strictly necessary, as this is a 1DOF simulation, but the 1DOF connection block did not work as intended. The middle plate and platform are attached with a spring and damper, with stiffness k_s and damping d_s, located in the middle of the plates. The platform has a limited workspace of ± 0.1 m. This is to simulate a limited work range, and the limits are taken the same as the travel range of the T-Flex in the z-direction. The contact between the ball and the platform is modelled by the

Circle to Finite Line block, from the Multibody Contact Force Library, which models a contact force between a circle and a finite line. The impact behaviour is characterised by the contact stiffness k_c and the contact damping d_c. The used force law is linear and no friction is assumed. Additionally, no air resistance is modelled.

The platform position and velocity in the world frame can be obtained by using the Transform Sensor block (the block denoted by S). The Circle to Finite Line block outputs the normal force between the ball and the platform. In the simulations, the contact force on an empty end-effector is strictly zero, so the time at which the impact starts is the time at which the contact force on the platform is not zero anymore. The end of the impact is when the contact force is zero again. The detectImpact variable is a boolean, to indicate whether a ball is on the platform.

The Measurements block takes the contact force, the end-effector position and the current time as input. At the moment that detectImpact is true, these values are saved into an array, which is stopped at the moment that detectImpact is false again. After the impact has finished, the linear impulse is calculated by piecewise constant integration of the contact force multiplied by the sample time. The Backward Estimation and Forward Estimation blocks estimate the ball trajectory as described in Section 3.5. Additionally, the COR is calculated in the Forward Estimation block for each collision. Since k_c, d_c, k_s and d_s all determine the impact behaviour, the COR varies for each combination of these, so one constant value for the COR would render incorrect results. The COR is used to calculate the platform velocity for the next bounce in the Generate Platform Trajectory block. This block is the implementation of Section 3.7 and after the generation and verification of the trajectory, it outputs the reference position for the platform for each time sample.

3.8.2 Results

In the simulations, the ball is dropped from a known height z'_{drop} with respect to the platform, which is indicated with the prime. After the first bounce, the platform trajectory is calculated and from the second bounce onward, the platform executes the calculated trajectories to achieve a constant bouncing height. The stiffness and damping of the spring and damper supporting the platform are varied, as well as the contact stiffness and damping, z'_{drop} and z_{ref}. This results in a total of 1728 different parameter combinations. The simulation time is 15 seconds. See Table 3.1 for the used variables.

Table 3.1: The used variables in the simulation for the one-directional bouncing. The left column contains the variables with a fixed value and the right column contains the variables whose value is varied.

Variable	**Value**	**Variable**	**Values**
t_s	1e-3 s	k_c	$[2000, 3000, 4000, 5000]$ N/m
r_b	0.0335 m	d_c	$[2, 3, 4]$ Ns/m
m_b	0.057 kg	k_s	$[1500, 2000, 2500, 3000]$ N/m
L_p	0.8 m	d_s	$[10, 20, 30]$ Ns/m
t_p	0.01 m	z'_{drop}	$[0.25, 0.5, 0.75, 1]$ m
w_p	0.4 m	z_{ref}	$[0.5, 0.75, 1]$ m
m_p	10 kg		
t_{sim}	15 s		
$z_{p,lim}$	$\pm 0.1m$		

The evaluation of the simulated bouncing is threefold. First, it is assessed in which cases the calculated platform trajectory is not feasible and ball bouncing fails. Next, the parameter estimations for $v_b^i[i]$, $v_b^o[i+1]$, $\hat{v}_b^i[i+1]$ and $\Delta\hat{t}$ are compared with the simulated values. Lastly, the error between the maximum ball height and the reference height is shown.

Feasibility of active bouncing
In some cases, the platform trajectory cannot be executed. This happens when the estimated time until the next bounce is shorter than the time it takes for the platform to complete the trajectory, or when the calculated trajectory exceeds the platform workspace. In the simulations, the active bouncing is assumed to have failed when the amount of bounces for a parameter combination is below ten. In other words, the platform could not execute the calculated trajectories and the bouncing of the ball eventually damps out. It is observed that this mainly occurs when the difference between z_{ref} and z'_{drop} is larger than 0.75 m. This combination of a low drop height and a high reference height requires a high platform velocity. With the fixed duration for the constant velocity, this results in a trajectory that exceeds the workspace limits and is therefore not executed. From the 1728 parameter combinations, 211 failed in sustained bouncing (12.2%).

Parameter estimation results
For the evaluation of the parameter estimation, the parameters of interest are $v_b^i[i]$, $v_b^o[i+1]$, $\hat{v}_b^i[i+1]$ and $\Delta\hat{t}$. These are, except for $v_b^o[i+1]$, the outputs of the backward estimation and forward estimation and they fully describe the ball trajectory. $v_b^o[i+1]$ is evaluated as well, as it is used in the calculation of both $\hat{v}_b^i[i+1]$ and $\Delta\hat{t}$. The calculated parameters are denoted with subscript *calc*. From the Transform Sensor blocks, the simulated values for the ball velocities can be obtained. For the time between bounces, the difference between the start of the impact and the end of the previous impact is taken. These are taken as the ground truth, indicated with subscript *gt*.

The estimations from the first bounce after the ball has been dropped have been discarded because the first backward estimation is altered and no trajectory is prescribed to the platform. Additionally, the predictions for $\hat{v}_b^i[i+1]$ and $\Delta\hat{t}$ have to be compared to measurements of the next bounce. The predictions that are done during the last bounce of one parameter set can therefore not be evaluated and are discarded. For this reason, there are fewer data points for these than for $v_b^i[i]$ and $v_b^o[i+1]$. Finally, only the simulations with sustained bouncing are considered.

The estimation error, here illustrated for the incoming ball velocity, can now be obtained by

$$\Delta v_b^i[i] = v_{b,gt}^i[i] - v_{b,calc}^i[i] \tag{3.16}$$

and the relative estimation error as

$$\tilde{v}_b^i[i] = \frac{\Delta v_b^i[i]}{v_{b,gt}^i[i]} \times 100\%. \tag{3.17}$$

The calculation is similar for $v_b^o[i+1]$, $\hat{v}_b^i[i+1]$ and $\Delta\hat{t}$.

The estimation errors and relative errors for $v_b^i[i]$, $v_b^o[i+1]$ are evaluated for 37250 bounces, shown in Figure 3.9. The prediction of $\hat{v}_b^i[i+1]$ and $\Delta\hat{t}$ is evaluated for 35737 bounces, which is shown in Figure 3.10.

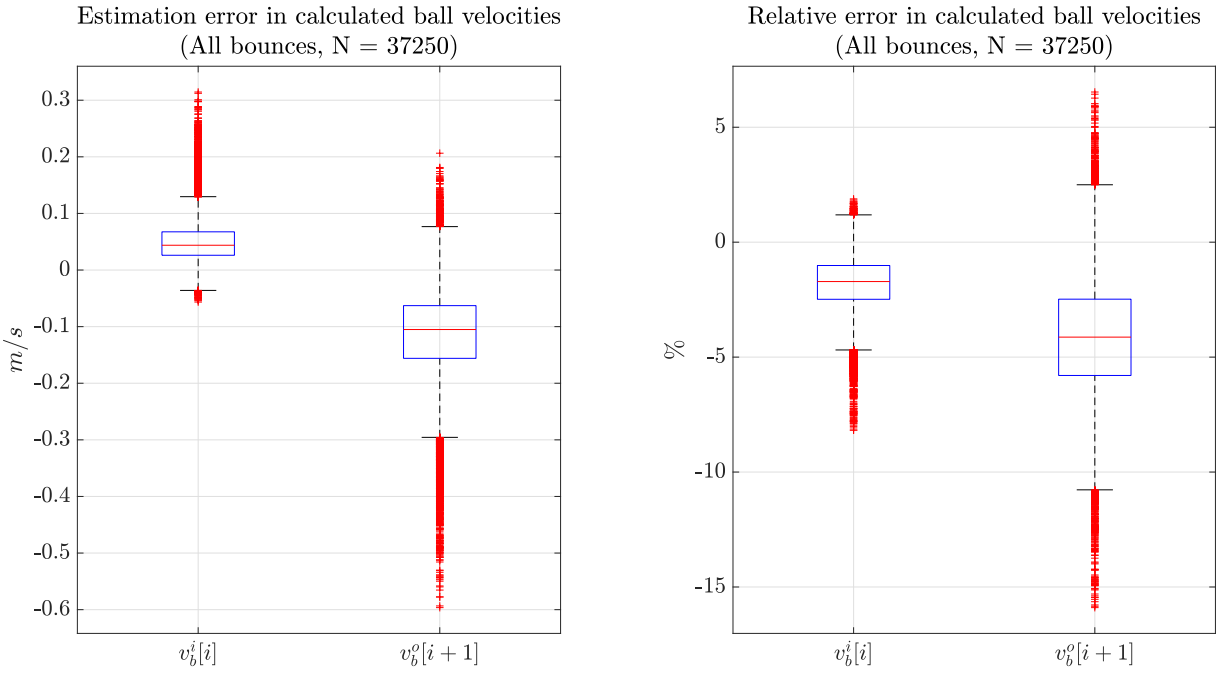

Figure 3.9: The estimation and relative errors for $v_b^i[i]$ and $v_b^o[i+1]$ in a one-dimensional bouncing simulation.

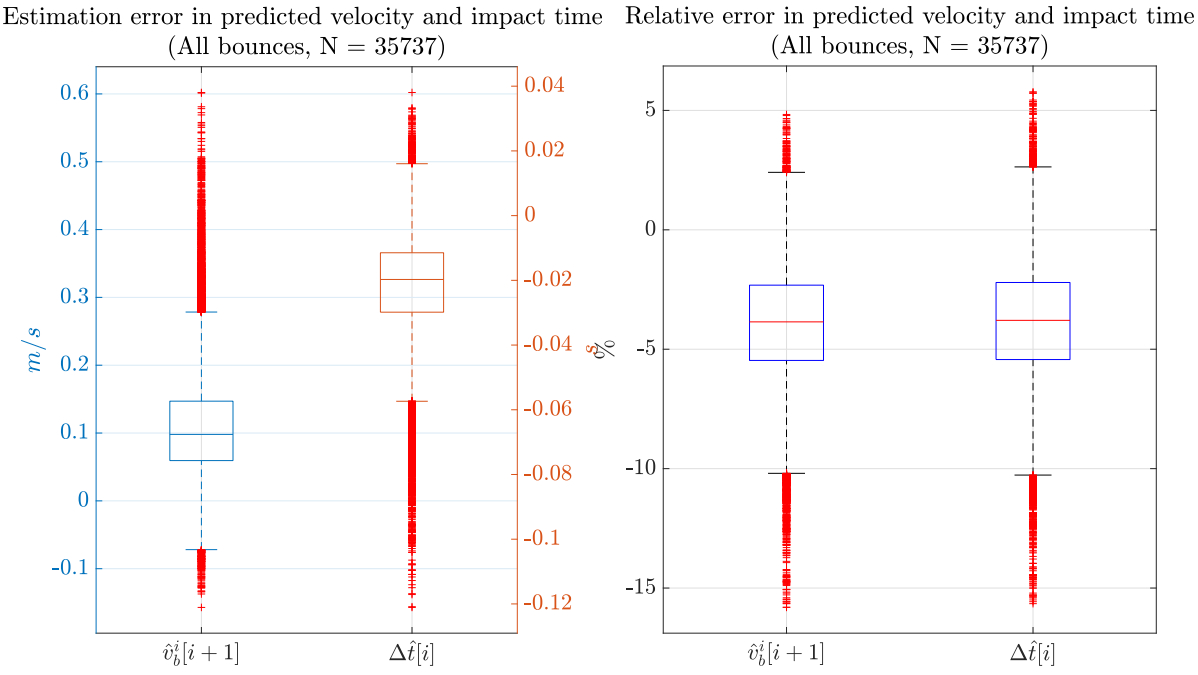

Figure 3.10: The estimation and relative errors for $\hat{v}_b^i[i+1]$ and $\Delta\hat{t}$ in a one-dimensional bouncing simulation.

It can be seen that $v_b^i[i]$ has a median relative error of -1.71% and $v_b^o[i+1]$ has a median relative error of -4.13%. The median estimation error for $v_b^i[i]$ is 0.04 m/s, and it is -0.11 m/s for $v_b^o[i+1]$. For reference, the median incoming velocity is -2.79 m/s and the median outgoing velocity is 2.78 m/s. For the relative error of $\hat{v}_b^i[i+1]$, a median of -3.85% is found, and for $\Delta\hat{t}$, this is -3.79%. The median estimation error is 0.1 m/s for $\hat{v}_b^i[i+1]$, and 0.02 s for $\Delta\hat{t}$. The average estimated velocity is -2.79 m/s, and the estimated time between bounces is 0.57 s. The distribution of the outliers in the relative error is similar for $v_b^o[i+1]$, $\hat{v}_b^i[i+1]$ and $\Delta\hat{t}$. This can be explained by the dependency of these variables on each other; $\Delta\hat{t}$ is calculated using $v_b^o[i+1]$ and $\hat{v}_b^i[i+1]$ is calculated using both $v_b^o[i+1]$ and $\Delta\hat{t}$. The variance in $v_b^i[i]$, which might be explained by its correction using Δt. Most outliers occur when there is a combination of a high contact stiffness and a high contact damping.

It can be seen that the distribution of the estimation error in $v_b^o[i+1]$ is larger than for $v_b^i[i]$. Since the estimation of $v_b^o[i+1]$ is also reliant on the measurement Δp, it is likely that the measurement contributes to the increased error distribution. The accuracy of the Circle to Finite Line block and its output (the contact force) does depend on the used solver, tolerances, sample time and used force law. A variable-step solver is recommended for the contact force library, but a fixed-step solver is used, because of the piecewise constant integration for the linear impulse. Additionally, the linear force law might be too simplified, compared to the available nonlinear or custom force law options. In the calculation of $\Delta\hat{t}$, it is assumed that the ball impacts exactly at the moment that the platform has the neutral position. This is not necessarily the case, which results in an error in the estimation of $\Delta\hat{t}$. Since the calculation of $\hat{v}_b^i[i+1]$ is dependent on both $v_b^o[i+1]$ and $\Delta\hat{t}$, these errors will propagate.

Control of the bouncing height

The objective of the bouncing model is to let the ball bounce to a given reference height. To assess the error between the reference height and the maximum bounce height, four scenarios are investigated. Here, the contact stiffness and reference height are varied, which results in the ball trajectories shown in Figure 3.11. The dashed line is the set reference, and the dotted lines are ±10% of the reference. It can be seen that for $z_{ref} = 0.5$ m, the settling time is longer when the contact stiffness is higher. For the same contact stiffness, but higher z_{ref}, the ball stays below 90% of the reference. In general, it is found that mainly a higher contact damping and a higher reference height result in a larger error. It should also be noted that the platform velocity is determined using a COR that is calculated during the previous bounce. Since that COR is not representative of the current bounce, the platform velocity might be higher or lower than required.

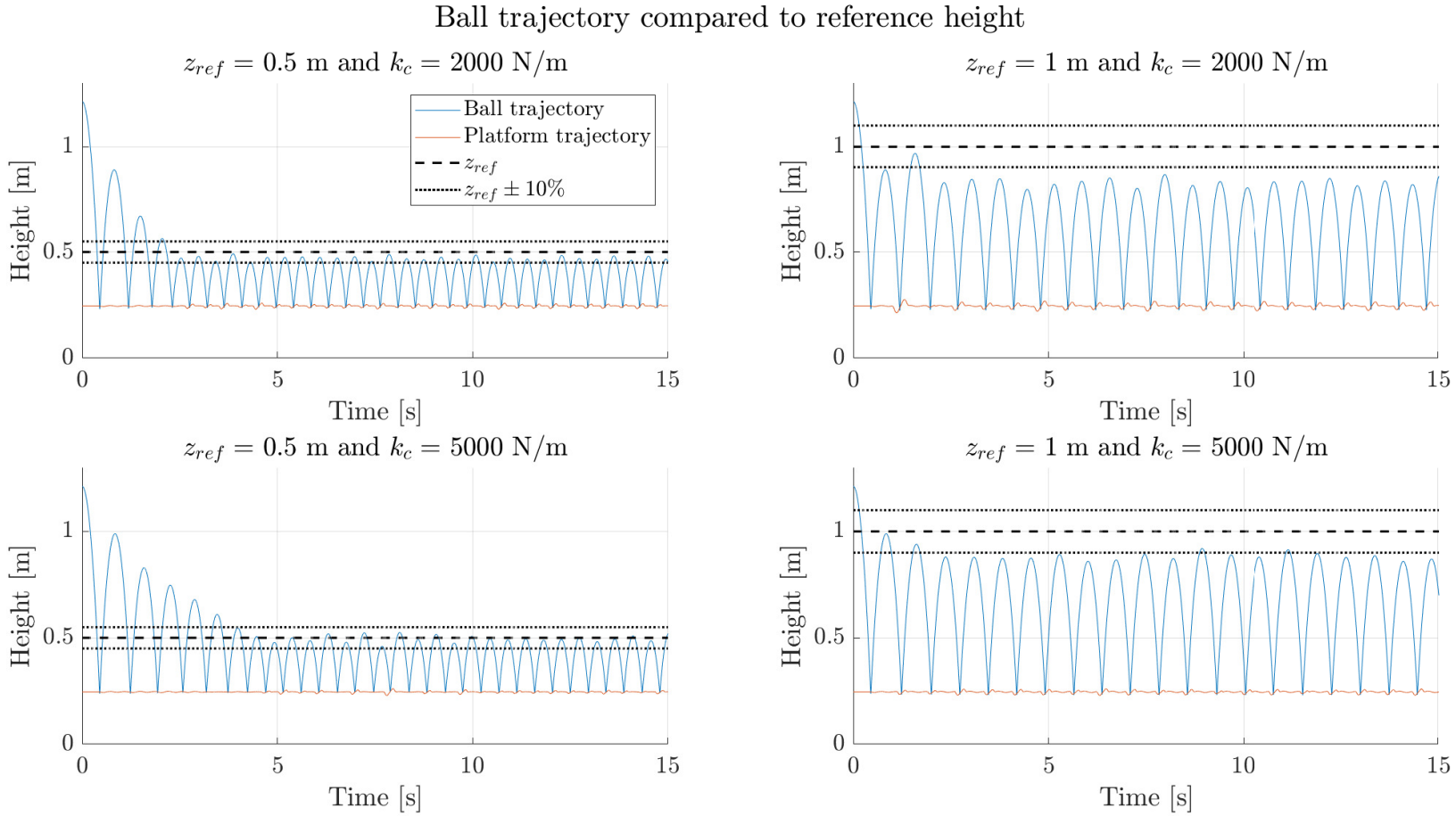

Figure 3.11: The ball trajectory in four active bouncing scenarios, compared to the set reference height. The contact stiffness and reference height are varied. For all four situations, the other variables are set to $d_c = 3$ *Ns/m,* $d_s = 20$ *Ns/m,* $k_s = 2000$ *N/m,* $z'_{drop} = 1$ *m.*

Chapter 4

2D Bouncing

4.1 Outline of the problem

The goal as described in Section 3.1 is unchanged. However, instead of bouncing in one dimension, the ball will now be bounced in two dimensions, resulting in sideways, in-plane bouncing. See Figure 4.1 for an illustration. The goal is to meet both a reference height and to direct the ball to a certain position on the platform. The ball can impact the platform on any position, not necessarily in the centre, and the platform can move in x-direction, z-direction and rotate around the y-axis.

4.1.1 Notation

The same notation as previously is adhered to. However, since the ball state is now two-dimensional, either a subscript is added to indicate the direction or the quantity is denoted as a vector.

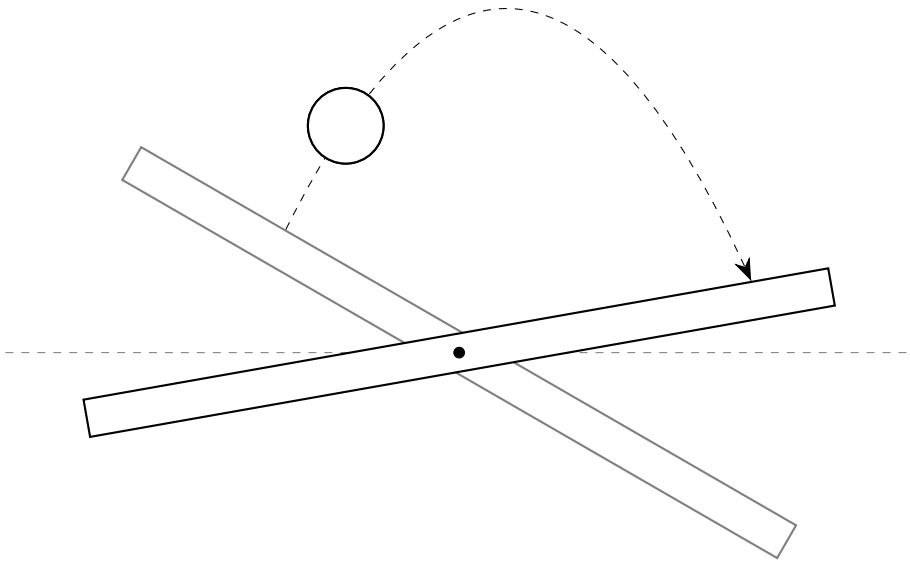

Figure 4.1: Illustration of two-dimensional bouncing. The ball bounces sideways and the aim is to achieve a given bouncing height and distance. In grey the platform position of the previous bounce, in black the platform position to bounce the ball to the next position.

4.2 Modelling of the ball impact

Analogously to the model as shown in Figure 3.3, a 2DOF model has been made, which is shown in Figure 4.2. The end-effector is again modelled as a mass, which is supported on the left and right edge by both a spring and damper. The left side is indicated with subscript l and the right side with r. The springs represent all stiffnesses that are present in the joints of the T-Flex as well as because of the PID controller. The dampers resemble the damping introduced by the PID controller and the electromagnetic damping. This 2D model is the basis for the simulations described in Section 4.8.

In this 2D model, the ball and platform can both translate in x- and z-direction. The ball is assumed not to spin, so all effects due to spin are neglected, but the platform can rotate around the y-axis. Air resistance is also neglected.

In Figure 4.2, free body diagrams of the platform and the ball are shown. The platform is initially at rest, with the gravitational force $F_{g,p}$ acting on it, as well as the modelled spring and damper forces, F_s and F_d. During impact, the ball hits at an arbitrary distance r from the centre of the platform. A contact force F_c acts on both the platform and the ball. The contact force on the ball is equal in magnitude but in the opposite direction of the contact force on the platform. Additionally, a tangential force F_t exists when the impact is oblique.

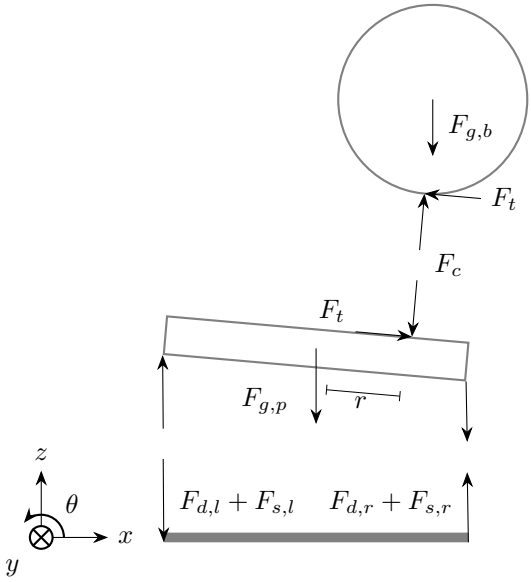

Figure 4.2: Free body diagrams of the ball and a 2DOF platform. The platform is supported by a spring and damper on both sides, and can rotate around the y-axis and move in x- and z-direction. The ball moves in x- and z-direction as well, but is assumed not to spin.

The equations of motion of the ball are

$$\begin{aligned} m_b a_{b,x} &= F_{c,x} - F_{t,x}, \\ m_b a_{b,z} &= F_{c,z} + F_{t,z} - F_{g,b} \\ I_b \alpha_b &= 0 \end{aligned} \tag{4.1}$$

where I_b is the inertia of the ball and α_b the angular acceleration. The last equation of motion is zero, because of the assumption of no ball spin.

4.3 Overview of the control scheme

In Figure 4.3, an overview is shown of the control scheme for the bounce height and distance. Given the measurements $\mathbf{\Delta p}$ and Δt, we would like to calculate the platform velocity $\mathbf{v_p}$, to bounce the ball to a given reference height z_{ref}, as well as a given location x_{ref}.

The control scheme is mostly similar to the one shown in Figure 3.4, except for some additional variables. Since the control problem is now two-dimensional, the positions, velocities and linear impulse are indicated as vector quantities. Additionally, a predicted angle of incidence $\hat{\beta}$ is calculated in the forward estimation. This $\hat{\beta}$ is the input for the controller C, which outputs the platform velocity $\mathbf{v_p}$, as well as a reference platform angle θ. Another output from the forward estimation is the estimated impact location of the ball $\hat{x}_b^i[i+1]$, which is input to the calculation of the reference velocity for the ball (CRV). Outputs of CRV are the ball reference velocity, $\hat{v}_{b,ref}^o$, and the reference angle of departure γ for the ball.

In the following sections, the calculations for the measurements and each block will be elaborated on.

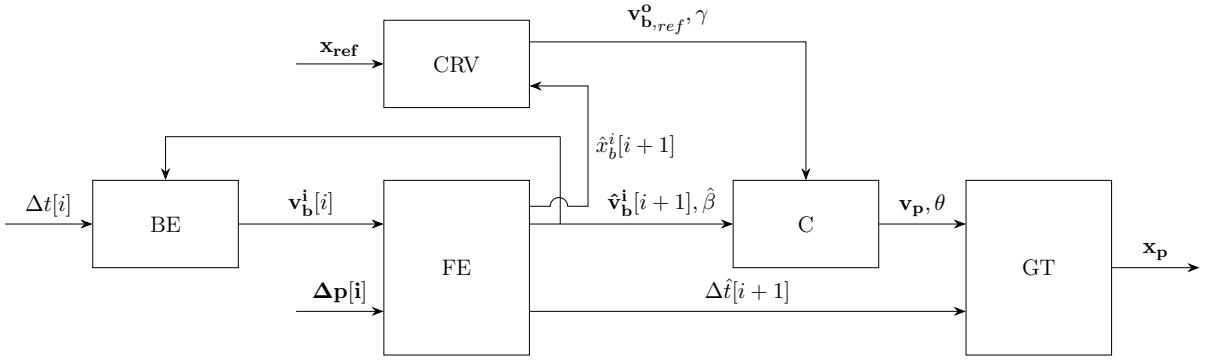

Figure 4.3: Block diagram for the control problem of bouncing a ball to a given reference height and location.

4.4 Obtaining measurements

In this section, the measurements of linear impulse and time between bounces are discussed. Additionally, an expression for the ball position on the platform and in the global frame is shown.

Obtaining the measurements for the time between two bounces is again as described in Section 3.4. Since the ball now might have a velocity in two directions, x and z, it also has linear momentum in two directions. For this reason, the linear impulse $\mathbf{\Delta p}$ can be expressed as a vector with components Δp_x and Δp_z.

As shown in Figure 4.2, there are both a normal contact force and a tangential force acting on the ball during impact, since the impact is oblique. Both can be decomposed into an x- and z-component, such that the linear impulses can be calculated as

$$\mathbf{\Delta p}[i] = \int_{t^i[i]}^{t^o[i+1]} m_b \mathbf{a_b}\, dt = \int_{t^i[i]}^{t^o[i+1]} \left(\mathbf{F_c} + \mathbf{F_t} - \begin{bmatrix} 0 \\ F_{g,b} \end{bmatrix} \right) dt. \tag{4.2}$$

Because the ball is assumed not to spin, its behaviour can be described by only using translational velocities. It is therefore sufficient to only consider the linear impulse and omit the angular impulse.

The distance r, from the contact point to the middle of the surface, is defined in the local frame as well, see Figure 4.2. r can be found by

$$r = -\frac{M_y}{\|\mathbf{F_c}\|}. \tag{4.3}$$

The measurement of the position of the ball is changed as well. The location of the centre of the ball in the global frame can be obtained using

$$\mathbf{x_b} = \mathbf{x_p} + (\frac{1}{2}t_p + r_b)\begin{bmatrix}\sin(\theta)\\ \cos(\theta)\end{bmatrix} + r\begin{bmatrix}\cos(\theta)\\ \sin(\theta)\end{bmatrix}, \tag{4.4}$$

where t_p is the thickness of the platform.

4.5 Estimation problem: ball trajectory prediction

In the two-directional bouncing, the trajectory of the ball is again parameterised by the velocities, but also by the bounce location of the ball on the end-effector. From the block scheme in Figure 4.3, it can be seen that the problem is again split in a backward and forward estimation. The backward estimation again takes $\Delta t[i]$ as input, and takes place right after the impact has started. The forward estimation has two inputs, the incoming ball velocity $\mathbf{v_b^i}[i]$, from the backward estimation, as well as the measured linear impulse. Therefore, the forward estimation happens when the impact has finished, and the calculations for the backward estimation are done. In this section, the calculations for the backward and forward estimations are presented. It is also shown how these are adjusted for the first bounce.

4.5.1 Backward estimation

At the moment of the backward estimation between bounce i and bounce $i+1$, the available measurement is $\Delta t[i]$. From the previous forward estimation, the prediction for the ball velocity $\hat{\mathbf{v}}_\mathbf{b}^\mathbf{i}[i]$ is known as well. The desired output for the backward estimation is the calculated incoming ball velocity $\mathbf{v_b^i}[i]$.

The velocity in x-direction can be calculated with the difference in x-position and the time between two bounces, while the velocity in z-direction can be found similarly to Equation (3.8), resulting in

$$\mathbf{v_b^i}[i] = \frac{1}{\Delta t[i]}(\mathbf{x_b^o}[i] - \mathbf{x_b^i}[i]) - \begin{bmatrix}0\\ \frac{1}{2}g\Delta t[i]\end{bmatrix}. \tag{4.5}$$

This calculated value of the ball velocity is used to correct the prediction of the ball velocity, by taking the average of the input $\hat{\mathbf{v}}_\mathbf{b}^\mathbf{i}[i]$ and the calculated value $\mathbf{v_b^i}[i]$.

4.5.2 Forward estimation

At the moment of the consecutive forward estimation, the measurement of $\mathbf{\Delta p}[i]$ is available. From the backward estimation, the input $\mathbf{v_b^i}[i]$ is obtained. The output for the forward estimation is the estimated impact time $\Delta\hat{t}[i+1]$, the predicted ball velocity for the next bounce

$\hat{\mathbf{v}}_\mathbf{b}^\mathbf{i}[i+1]$, the predicted angle of incidence $\hat{\beta}$ and the predicted location of impact $\hat{x}_b^i[i+1]$.

Since momentum is conserved in particular directions, the outgoing ball velocity in both directions can be calculated using the law of conservation of momentum. The outgoing velocities become

$$\mathbf{v}_\mathbf{b}^\mathbf{o}[i+1] = \frac{1}{m_b}\mathbf{\Delta p} + \mathbf{v}_\mathbf{b}^\mathbf{i}[i]. \tag{4.6}$$

The expression for the estimated impact time can be derived as shown in Section 3.5.2, resulting in

$$\Delta\hat{t}[i+1] = \frac{v_{b,z}^o[i+1]}{g} + \sqrt{\left(\frac{v_{b,z}^o[i+1]}{g}\right)^2 + \frac{2}{g}(z_b^i[i+1] - z_b^o[i+1])}. \tag{4.7}$$

where $z_b^o[i+1]$ is again chosen as the neutral position of the end-effector.

The predicted incoming ball velocity can now be found. With the assumption of no air resistance, the predicted incoming velocity $\hat{v}_{b,x}^i[i+1]$ is the same as the calculated outgoing velocity $v_{b,x}^o[i+1]$. Since the velocity in z-direction is subject to gravitational forces, the prediction becomes

$$\hat{\mathbf{v}}_\mathbf{b}^\mathbf{i}[i+1] = \mathbf{v}_\mathbf{b}^\mathbf{o}[i+1] - \begin{bmatrix} 0 \\ g\Delta\hat{t}[i+1] \end{bmatrix}. \tag{4.8}$$

To direct the ball to its reference bounce location, the ball should be intercepted with a correctly tilted platform. To this end, the estimated angle of incidence $\hat{\beta}$ and the estimated x-position of the ball during the next impact are relevant. The angle of incidence is the angle between the horizontal and the trajectory of the ball, see Figure 4.4. A vertically falling ball has an angle of incidence $\beta = \pi/2$. The angle of incidence can be calculated as

$$\hat{\beta} = \frac{\pi}{2} - \arctan\left(\frac{\hat{v}_{b,x}^i[i+1]}{\hat{v}_{b,z}^i[i+1]}\right). \tag{4.9}$$

Finally, the estimated x-position $\hat{x}_b^i[i+1]$ is calculated. This parameter is used in the calculation of the platform angle during impact. $\hat{x}_b^i[i+1]$ is calculated as

$$\hat{x}_b^i[i+1] = x_b^o[i+1] + v_{b,x}^o[i+1]\Delta\hat{t}[i+1]. \tag{4.10}$$

4.5.3 Estimation of first bounce

At the start of the bouncing sequence, limited information is available, similarly as described in Section 3.5.3. The ball is again released from a known height z_{drop}, which is set by the user, and falls vertically, such that the horizontal velocity is zero. The first measured time between two bounces is $\Delta t[2]$, as $\Delta t[1]$ cannot be measured. The first backward estimation is therefore again slightly adjusted. Now, the incoming velocity of the ball can be calculated using the law of conservation of energy, as

$$v_{b,z}^i[1] = -\sqrt{2g(z_{drop} - z_b^i[1])}. \tag{4.11}$$

During the first collision, $\Delta p[1]$ is measured, and the distance r, between the impact location and the center of the platform can be found as well, as in Equation (4.3). With this information, all calculations in the first forward estimation can be done. Hereafter, all backward and forward estimations can take place as described previously.

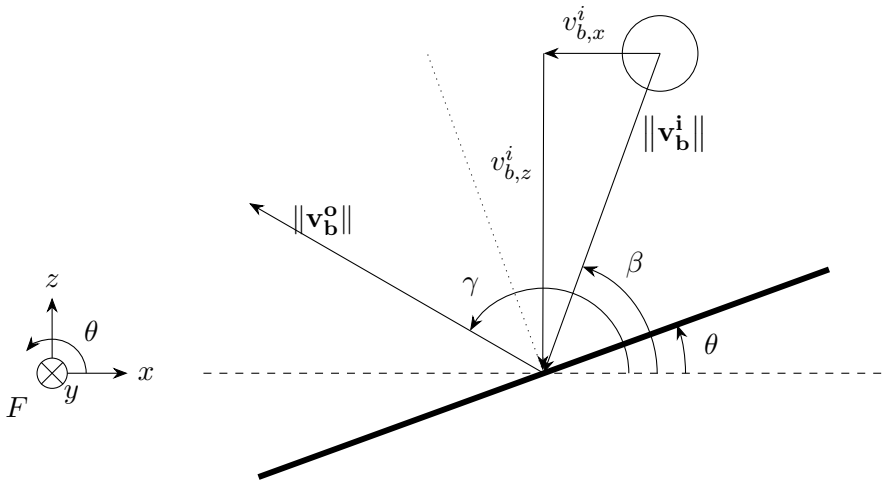

Figure 4.4: The angle of incidence β, the angle of departure γ and the angle of the platform θ. All angles are defined with respect to the horizontal, shown as the dashed line.

4.6 Control problem: height and distance regulation

Using the estimated ball velocities, impact location and angle of incidence, a control input for the ball can be found. The control input for two-dimensional bouncing consists of a platform velocity in x- and z-direction. In this section, the derivation thereof is shown.

For the 2D bouncing, it is necessary to obtain a certain reference height, z_{ref} as well as a certain bouncing location x_{ref}. Both are necessary to calculate the reference ball velocity, $\mathbf{v_{ref}}$, which is represented by the CRV block in Figure 4.3. The inputs for this block are the references, as well as the estimated ball impact location $\hat{x}^i_b$ from the forward estimation.

The difference between the outgoing position of the ball and its reference position can be denoted by

$$\begin{aligned} \Delta x &= x_{ref} - x^o_b \\ \Delta z &= z_{ref} - z^o_b. \end{aligned} \tag{4.12}$$

Since x^o_b is unknown, is chosen to be equal to $\hat{x}^i_b$, under the assumption that the ball does not roll or slide during the impact. z^o_b is once again chosen to be the neutral position of the platform, to be coherent with the estimation of $\Delta\hat{t}[i+1]$ and the design of the robot trajectory.

These distances Δx and Δz are related to each other by the angle of departure γ. When the horizontal distance that needs to be covered is longer, a lower maximum height can be achieved, and vice versa. This relation can be derived from the expressions for the maximum height and the expression for the distance that is covered during the flight, as shown in Appendix D. From the derivation, it follows that these three properties are related to each other by

$$\frac{\Delta z}{\Delta x} = \frac{\tan(\gamma)}{4}. \tag{4.13}$$

For stable bouncing, it is required that the ball always flies upward. Therefore, it must hold that $0 < \gamma < \pi$. Δz is always positive and Δx is either positive, negative or zero, depending on where the ball lands and what the reference location is. Since the arctan function is undefined

for $\Delta x = 0$, the atan2 function is better suited. Now, γ can be calculated as

$$\gamma = \text{atan2}(4\Delta z, \Delta x). \tag{4.14}$$

From the expression for Δz as derived in Equation (D.14), it is possible to calculate the reference for the absolute ball velocity. The reference ball velocity is calculated as

$$\|\mathbf{v_b^o}\| = \frac{\sqrt{2g\Delta z}}{\sin(\gamma)}. \tag{4.15}$$

This reference ball velocity is the input for the controller C.

The other inputs for the controller C are the estimated angle of incidence and the reference angle of departure. Its output is the platform velocity. According to [28], the absolute platform velocity can be calculated from the reference ball velocity and estimated incoming velocity, as

$$\|\mathbf{v_p}\| = \frac{\|\mathbf{v_b^o}\|}{e} - \left\|\mathbf{v_b^i}\right\|. \tag{4.16}$$

Finally, to obtain the separate x- and z-components of the velocity, the angle θ that the platform should make with respect to the horizontal, can be calculated as well. The derivation of this is shown in Appendix E. This relation is

$$\theta = \frac{\gamma + \beta - \pi}{2}. \tag{4.17}$$

Combining Equation (4.16) and Equation (4.17), the x- and z-components of the platform velocity are found as

$$\begin{aligned} v_{p,x} &= \|\mathbf{v_p}\| \sin(\theta), \\ v_{p,z} &= \|\mathbf{v_p}\| \cos(\theta). \end{aligned} \tag{4.18}$$

4.7 Platform trajectory generation

From the estimated impact time, found in the forward estimation, and the platform velocities, from the controller, a position profile for the platform can be obtained. Contrary to the platform trajectory generation for the 1D bouncing, now three trajectories have to be generated: for x, z and θ.

For the trajectory in x- and z-direction, the trajectory generation is exactly as described in Section 3.7. The trajectory for both directions is generated separately, therefore the time at which the trajectories start may differ (i.e. the movement in x-direction might start later than the movement in z-direction, or vice versa). In both directions, the same maximum acceleration, workspace limits and duration of the constant velocity are used.

In addition to the translation of the platform, a rotation is required as well. Here, the rotation, and not the rotational velocity, is required to stay constant during the impact. Therefore, this trajectory is constructed slightly differently from the translational trajectories.

In Figure 4.5, an image is shown of a generalised trajectory for the angle. The platform starts at time t_1 with an angle of $\theta_1 = 0$. The ball is expected to impact the platform at time t_i and the interval over which a constant angle is required, is taken as 2σ. This results in values for t_3 and t_4 are therefore the same as those calculated in Section 3.7. The rest of the calculation of the trajectory is shown in Appendix F. After the generation of the profile for the angular motion, it can be verified whether it is within the allowed workspace and whether the trajectory is feasible in the available time.

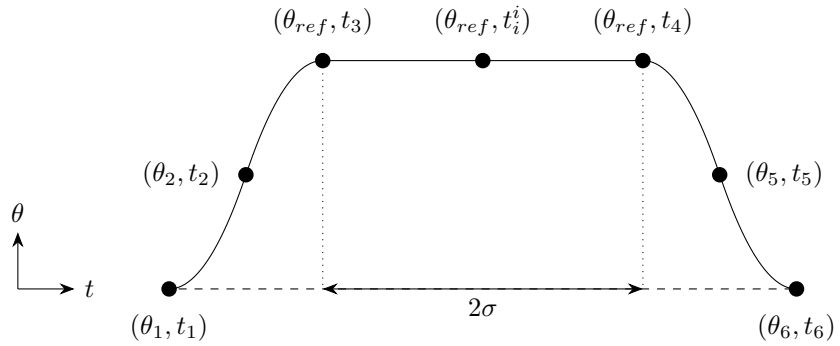

Figure 4.5: Generalised image of the angular platform trajectory over time, to do two-dimensional bouncing. The expected impact time of the ball on the platform is t_i^i. The platform has a constant angle θ_{ref} for a duration of 2σ, between t_3 and t_4. Here, σ is the estimation error of t_i^i.

4.8 Simulations

The simulation for one-dimensional bouncing has been extended to a simulation for two-dimensional bouncing, to verify the theoretical framework. One simulation is presented as proof of concept. Next, the results of this are shown and discussed.

4.8.1 Simscape model

An image of the simulation set-up is shown in Appendix G. The model as shown in Figure 4.2 is used as the basis for this simulation. The properties and DOFs of the ball are kept the same as in the 1D simulation. The platforms have the same properties as well, but the middle plate now has 3 DOFs with respect to the ground: translation in x- and z-direction and rotation around the y-axis. A position profile can be prescribed for all three DOFs. The connection between the middle plate and the platform is changed to a spring and damper on both sides, with stiffness k_s and damping d_s. The platform has a limited workspace of ± 0.1 m in both x- and z-direction and $\pm 11.5°$ for θ. The modelling of the ball flight and impact behaviour is unchanged. The COR is now calculated using all absolute velocities.

The contact between ball and platform is again modelled using the Circle to Finite Line block, which is able to output the contact forces in x- and z-direction, in the global frame. Additionally, the moment imposed on the platform due to contact is obtained from this block as well. The exact moment of the start and end of the impact is determined by comparing F_c to 0, similarly as in the one-dimensional simulation, which results in the boolean detectImpact.

The Measurements block takes the contact forces, the end-effector position and the current time as input. At the moment that detectImpact is true, these values are saved into an array, which is stopped at the moment that detectImpact is false again. After the impact has finished, the linear impulses are calculated by piecewise constant integration of the contact force multiplied by the sample time t_s. The Backward Estimation and Forward Estimation blocks estimate the ball trajectory as described in Section 4.5. The Generate Platform Trajectory block is the implementation of Section 4.7 and after the generation and verification of the trajectory, it outputs the x, z and θ reference position for the platform for each time sample.

The simulation is not fully working as intended yet. It is not robust for certain combinations of stiffness and damping, drop height and references. It has not been investigated yet whether

this is due to an implementation error or if two-dimensional bouncing is indeed only feasible for a limited range of these variables. Therefore, only one simulation is done, as a proof of concept and to point out certain issues with the current simulation.

4.8.2 Results

The ball is dropped from a height z'_{drop} and location x'_{drop} with respect to the platform. After the first bounce, the platform trajectory is calculated and from the second bounce onward, the platform executes the calculated trajectories. In Table 4.1, the used variables are shown. The reference in the x-direction changes, depending on the landing position of the ball. It can be described as

$$x_{ref} = \begin{cases} -0.05 & \text{if } x_b^i \geq 0.05 \\ 0.05 & \text{if } x_b^i < -0.05. \end{cases} \tag{4.19}$$

Table 4.1: The used variables in the simulation for the two-directional bouncing.

Variable	**Value**	**Variable**	**Value**
t_s	1e-3 s	k_c	1500 N/m
r_b	0.0335 m	d_c	1 Ns/m
m_b	0.057 kg	k_s	1000 N/m
L_p	0.8 m	d_s	10 Ns/m
t_p	0.01 m	z'_{drop}	1.5 m
w_p	0.4 m	z_{ref}	0.75 m
m_p	10 kg	x'_{drop}	0.1 m
t_{sim}	30 s		
$x_{p,lim}, z_{p,lim}$	$\pm 0.1m$		
θ_{lim}	$\pm 11.5°$		

First, the estimation of several parameters will be compared with the simulated values. Next, the ball trajectory will be evaluated for how well both references are tracked and some observations are made with regard to the ball trajectory.

Parameter estimation results
For the parameter estimation, the parameters that are evaluated are $v_{b,x}^i[i]$, $v_{b,z}^i[i]$, $\hat{v}_{b,x}^i[i+1]$, $\hat{v}_{b,z}^i[i+1]$, $\hat{x}_b^i[i+1]$ and $\hat{\beta}[i+1]$. These are outputs of the backward and forward estimation and the predicted values for the velocity, impact location and angle of incidence determine the control of the ball trajectory. From the Transform Sensor blocks, the simulated values for the ball velocities and position can be obtained. The true value for β is obtained by using the measured velocities in Equation (4.9).

Similar to the one-dimensional simulations, the estimations for the first bounce are discarded. Additionally, the last value of the predicted values is omitted because it cannot be compared to a measured value. This leaves 41 bounces.

The relative errors for all parameters are shown in Figure 4.6. The parameters $v_{b,x}^i[i]$, $v_{b,z}^i[i]$, $\hat{v}_{b,x}^i[i+1]$ and $\hat{v}_{b,z}^i[i+1]$, all show one major outlier, but it is not from the same bounce. It can be observed that the prediction for $\hat{x}_b^i[i+1]$ and $\hat{v}_{b,x}^i[i+1]$ have a larger distribution of the error compared to the other parameters, but it is unclear what is causing this.

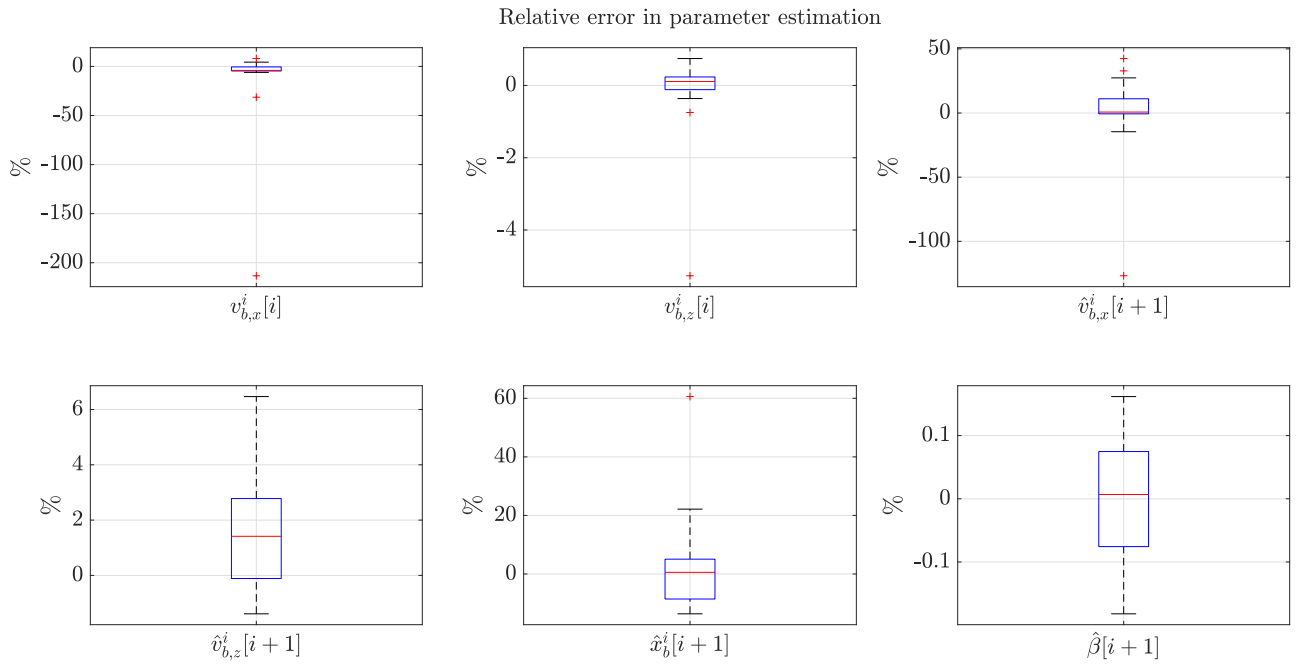

Figure 4.6: Relative errors in the estimated parameters for the simulated two-dimensional bouncing.

Control of the bouncing height and location

The ball trajectory is shown in Figure 4.7. In blue, the x-position of the ball is shown and in orange the z-position. The ball bounces from left (negative x-value) to right (positive x-value). It can be seen that the maximum height of the ball overshoots the reference in some bounces, but in general stays within ±10% of the reference. The landing position of the ball is in general close to the given reference.

It can be observed that the ball often makes an intermediate bounce. For some bounces from left to right however, the bounce does succeed immediately, e.g. around 6 s and 19 s. It can be observed that a bounce with a larger relative error for $\hat{x}^i_b[i+1]$ and $\hat{v}^i_{b,x}[i+1]$ ($> \pm 5\%$) is followed by an intermediate bounce, but it is unknown whether this is also the cause for the intermediate bounce.

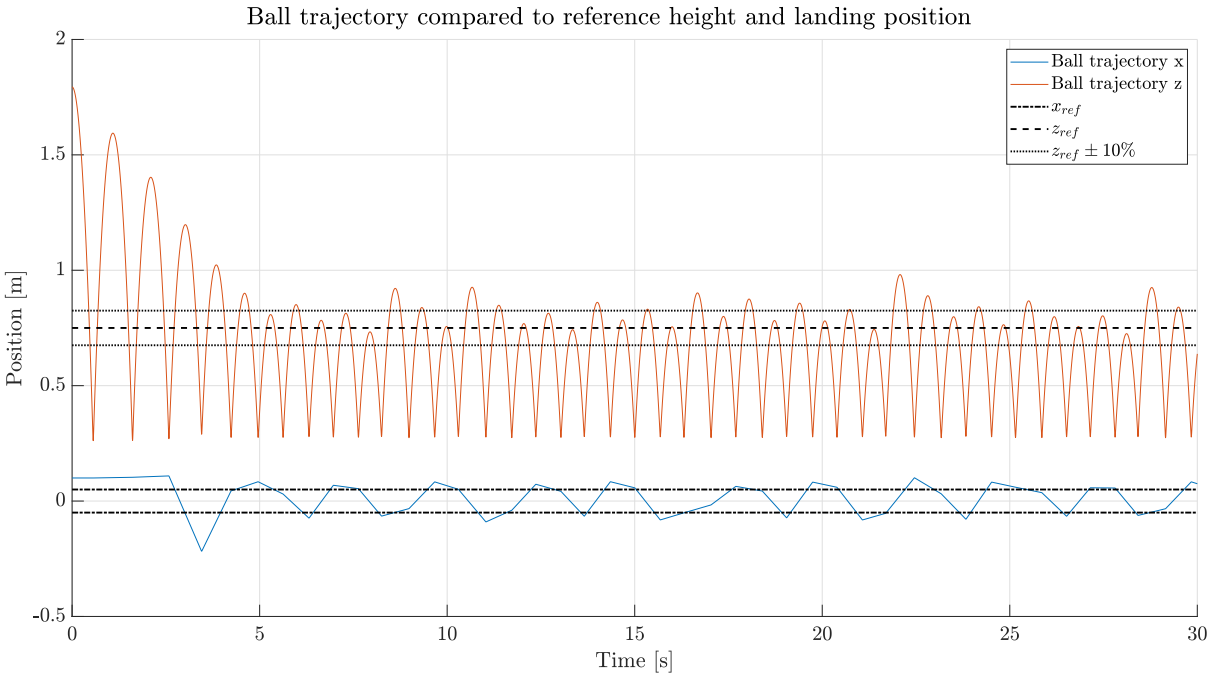

Figure 4.7: The ball trajectory in x- and z-direction, compared to the references for both directions.

Chapter 5

Emperical results and feasibility

The theoretical framework for one-dimensional bouncing has been verified experimentally on the T-Flex. First, a method for estimation of the contact force between the ball and the platform is established and verified. It is shown that the impact location can be found using the contact forces and moments. A different parameterisation of the ball trajectory is developed, as the one that was established previously appeared to be unrepresentative of the real set-up. The derived relations for the ball height and measurements are verified on the T-Flex. Finally, a feasibility analysis for bouncing a ball on the T-Flex is conducted, to show the potential of ball bouncing.

5.1 The T-Flex

The T-Flex is a flexure-based hexapod, with six degrees of freedom. It is equipped with six direct drive actuators at its base, the Tecnotion QTR-A-133-60-N torque motors. The controller for the actuators is a Kollmorgen servo drive of type AKD-P00306. It delivers current feedback with a resolution of 1 mA, which results in torque feedback with a 6 Nmm resolution. This translates to a resolution of 0.00314 N at the end-effector in neutral position. The encoders are of type Heidenhain LIC 4119, which have a resolution of 13 nrad, which is 6.8 nm at the end-effector. More details on the T-Flex and its components can be found in [1].

The global frame F is located at the middle of the base, between the actuators, see Figure 5.1. In addition, a local frame F' is defined, which is located at the middle of the end-effector. From here on, the ball position is expressed in this local end-effector frame. The neutral position of the end-effector is at $[0, 0, 0.29]$ m, in the global frame. This is the reference position for the platform when no position profile is issued and it is the position that the platform has at the predicted time of impact in the case of active bouncing.

5.2 Estimation of the contact force

To implement the parameter estimation as presented in Section 3.5 on the T-Flex, the contact force is required. In this section, a method for estimating the contact force on the end-effector is presented.

The torque feedback of the actuators returns a measured torque $\boldsymbol{\tau}_{meas}$, which is the amount of torque that was delivered by the actuators. Additionally, the inverse dynamics model of the T-Flex is known, which gives the actuator torques required to actuate the modelled, nominal system [51]. These calculated actuator torques are here named estimated torque $\boldsymbol{\tau}_{est}$. Any

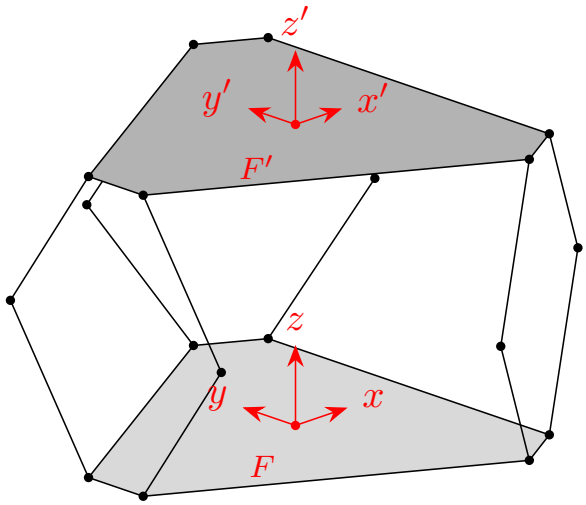

Figure 5.1: Schematic drawing of the T-Flex with the global frame F and the local frame F'. The global frame is placed in the middle of the base, the local frame is located in the middle of the end-effector.

torque that is unmodelled, such as noise, uncertainty and torque due to impact, is not included in this estimation. This unmodelled torque, $\boldsymbol{\tau}_{diff}$, can therefore be obtained by comparing this estimation with the measured actuator torque, as

$$\boldsymbol{\tau}_{diff} = \boldsymbol{\tau}_{meas} - \boldsymbol{\tau}_{est}. \tag{5.1}$$

In tests with non-adaptive feedforward the feedback torque is 18.5 Nmm [51], which translates to 0.00968 N on the end-effector in neutral position. With an impact of a tennis ball with a mass of 0.057 kg falling from 1 m height and an impact duration of 0.018 s, the contact force is approximately 27.5 N. Here, it is assumed that the maximum force occurs halfway through the impact. It can therefore be assumed that the difference is only due to the impact. The torque difference of the actuators can be transformed to the local frame on the end-effector, resulting in the contact forces and moments, as

$$\mathbf{F_c} = J^T \boldsymbol{\tau}_{diff}, \tag{5.2}$$

where J is the Jacobian matrix from the actuator angles to end-effector coordinates.

This method for contact force estimation has been verified using standard weights of 100 and 200 gram. First, the platform is moved to its neutral position, where it is held. Then, the weight of 200 gram is placed and after several seconds, the weight of 100 gram is placed next to it. Next, both weights are removed, first the 100 gram weight and several seconds later the 200 gram weight. This sequence is repeated multiple times, first in two of the corners, then the middle and finally the last corner. The estimation of the contact forces and moments is shown in Figure 5.2.

It can be observed that over time, an offset occurs, mainly with the force and moment in z-direction. It is suspected that this is due to Dahl hysteresis model that is used in the inverse dynamics. It can be assumed that the drift is negligible during the impact, because of its short duration. Therefore, the contact force estimation is still accurate for differential measurements.

To evaluate the correctness of the contact force estimation, it is considered whether the increase or decrease of the contact force corresponds with the increase or decrease of mass on the

platform. The mean absolute error for the weights of 100 gram is 0.0037 kg (3.7% relative error) and 0.0065 kg for the weight of 200 gram (3.23% relative error).

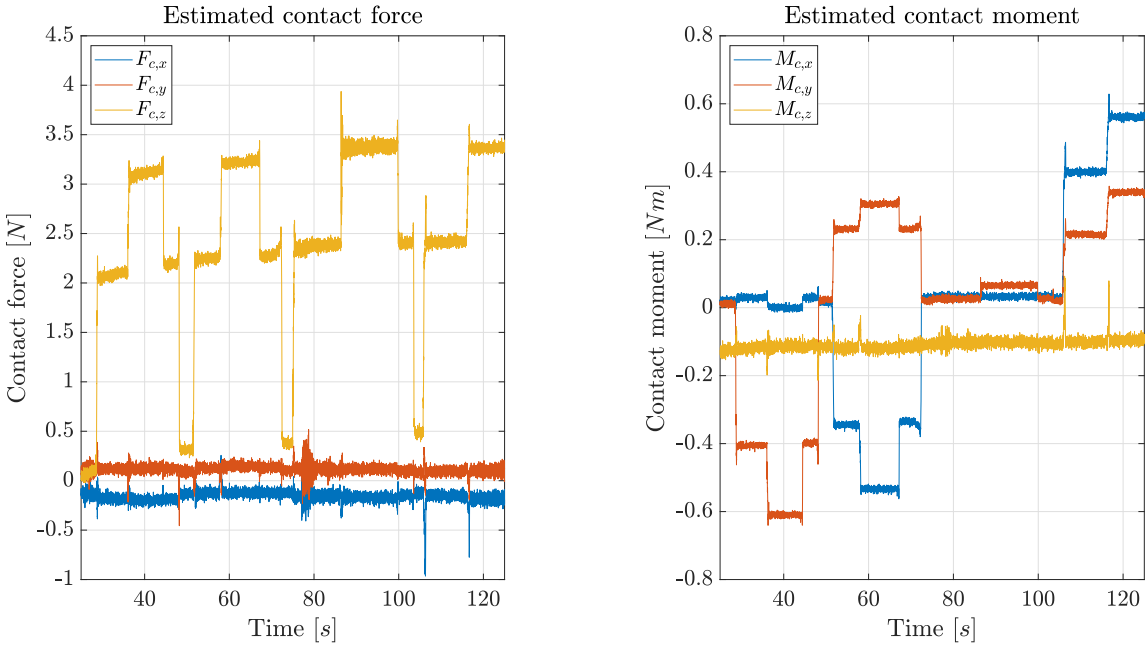

Figure 5.2: Estimated contact forces and moments on the T-Flex, using standard weights of 100 and 200 gram.

5.3 Estimation of the impact location

The impact location $\mathbf{r}$ is the distance of the impact from the centre of the platform, expressed in end-effector frame F'. It can be found using the estimated contact forces and moments by solving the relation

$$\begin{bmatrix} 0 & -F_{c,z} \\ F_{c,z} & 0 \end{bmatrix} \begin{bmatrix} r_x \\ r_y \end{bmatrix} = \begin{bmatrix} M_{c,x} \\ M_{c,y} \end{bmatrix}. \tag{5.3}$$

for r_x and r_y. The estimation of the loading locations from Figure 5.2 has been shown in Figure 5.3. The correctness of the estimation has not been quantified, but the estimated locations did approximately correspond to the locations where the weights are placed. Although the impact location is not required in one-dimensional bouncing, it is required when two- or three-dimensional bouncing is implemented.

5.4 Development of a new ball trajectory formulation

In the following section, it will be shown that the parameter estimation that was shown and validated in Section 3.5 returns inaccurate results. To gain more insight, the ball trajectory and measurements are now parametrised using the bounce height and the platform velocity. Analytical relations for the next bounce height and the measurements are derived.

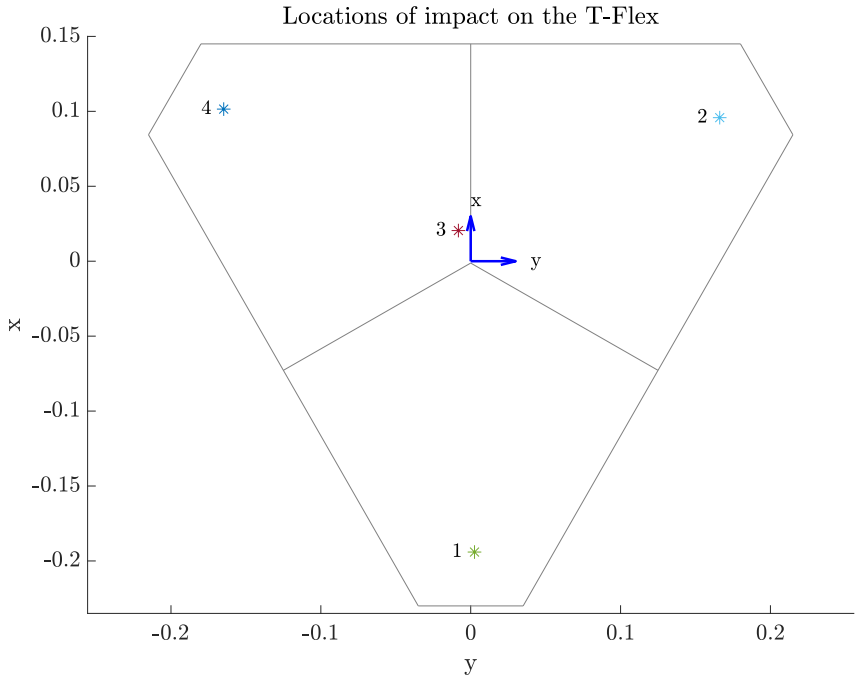

Figure 5.3: Estimated locations of the weight on the T-Flex, from the experiment in Section 5.2. In grey the top view of the end-effector of the T-Flex.

5.4.1 Motivation for the alternative formulation

The parameter estimation procedure that was developed in Section 3.5, showed poor performance in the estimation of the parameters on the T-Flex during preliminary tests. In Figure 5.4, an estimation of the ball height is shown for a single experiment. The ball was dropped from 0.25 m above the end-effector. On the horizontal axis, the ball height as observed using a camera is plotted. In blue, a calculation of the ball height using Δt is shown, where the calculation is

$$z_b^m[i] = \frac{g}{8}(\Delta t)^2. \tag{5.4}$$

Here, it is assumed the ball reaches its maximum height at $\frac{1}{2}\Delta t$. In red, a calculation of the height using Δp is shown, where the calculation is

$$\begin{aligned} v_b^o[i] &= \frac{\Delta p}{m_b} + v_b^i[i-1], \\ z_b^m[i] &= \frac{(v_b^o[i])^2}{2g}. \end{aligned} \tag{5.5}$$

This relation for $z_b^m[i]$ is obtained from the conservation of energy. It can be seen that the calculation using Δp deviates strongly, while the calculation using Δt seems to coincide with the camera observation. This was observed for multiple bounces, and also from different heights. This gives reason to assume that either the measurement of Δp is incorrect, or that the parameter estimation as established in Section 3.5 is incorrect or uses invalid assumptions.

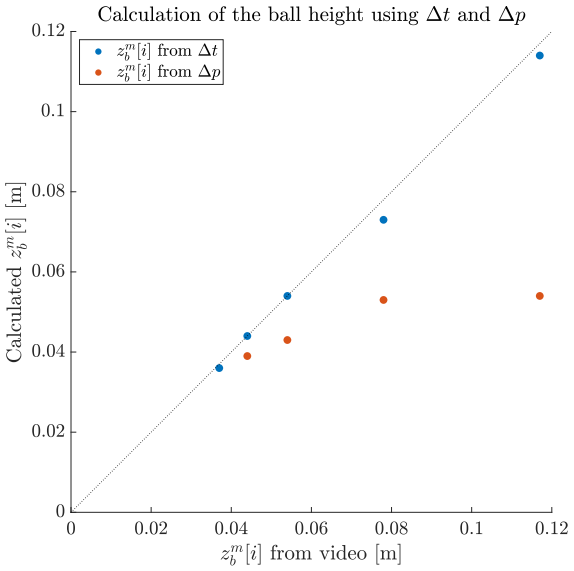

Figure 5.4: Calculation of the ball height using the measurements of Δt and Δp, compared to the ball height observed from camera measurements.

5.4.2 Derivation of analytical relations

An alternative parametrisation is developed to gain more insight into how and why the parameter estimation fails and to potentially obtain a better parameter estimation. The new approach uses a state-space representation similar to that of a Kalman filter. Therefore, the measurements Δt and Δp can be compared against a measurement model and both can be used to correct the prediction of the ball prediction. Previously, only Δt was used for corrections. The ball trajectory and the measurements Δt and Δp will now be parameterised using only the ball height as a state and platform velocity as an input. See Figure 5.5 for an overview. The ball velocity is directly related to the maximum height, by the conservation of energy, where it is assumed that there is no air resistance. Additionally, the velocity and height of the ball are influenced by the platform velocity during impact. Using the equations that describe these relations, it is possible to fully express the ball trajectory using the maximum height z_b^m as the state variable and the platform velocity v_p as the control input. A similar relation can be found for the measurements Δt and Δp. It appears that Δt is only dependent on $z_b^m[i]$, while Δp is determined by both $z_b^m[i]$ and v_p.

By describing the physical process and the measurements as described above and taking into account the uncertainty, or noise, n, a generic description of the relations can be found as

$$\begin{aligned} z_b^m[i+1] &= f(z_b^m[i], v_p) + n_f \\ \Delta t &= g(z_b^m[i]) + n_g \\ \Delta p &= h(z_b^m[i], v_p) + n_h. \end{aligned} \tag{5.6}$$

In the following, an expression for the functions f, g and h is derived using physics-based relations.

Derivation of predictor $\mathbf{z_b^m[i+1]}$
First, the predictor for $z_b^m[i+1]$ is derived. The relation for the COR as described in Equation (3.1) is used, as well as the assumption that the platform velocity remains constant during

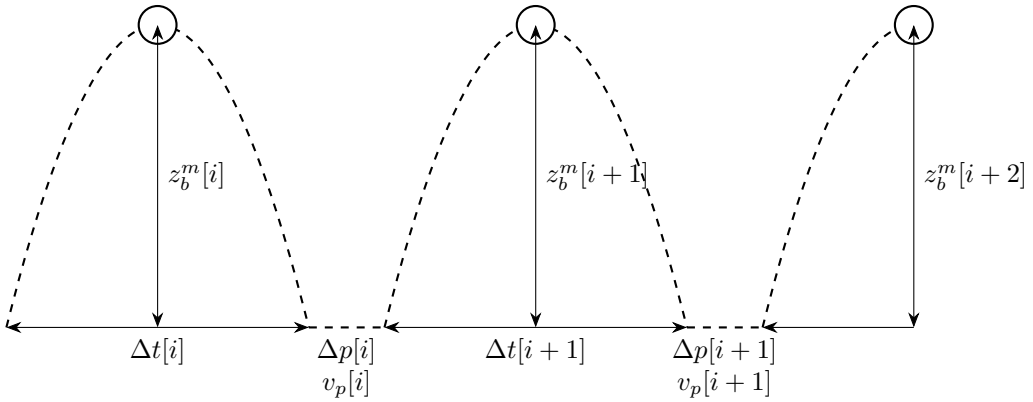

Figure 5.5: Schematic representation of the ball trajectory and the parameterisation of it. The measurements during the impact are indicated.

impact. This results in

$$v_b^o[i+1] = (1+e)v_p - ev_b^i[i]. \tag{5.7}$$

By the assumption that there is no air resistance, so all kinetic energy is converted to potential energy, this relation can be extended to

$$\sqrt{2g(z_b^m[i+1] - z_b^o[i+1])} = (1+e)v_p + e\sqrt{2g(z_b^m[i] - z_b^i[i]))}. \tag{5.8}$$

Finally, this can be rewritten to an expression for $z_b^m[i+1]$, which gives

$$z_b^m[i+1] = \frac{\left((1+e)v_p + e\sqrt{2g(z_b^m[i] - z_b^i[i])}\right)^2}{2g} + z_b^o[i+1]. \tag{5.9}$$

Derivation of measurement Δt

Next, the measurement of Δt can be modelled using the assumption that the maximum height of the ball is achieved at $\frac{1}{2}\Delta t$. The trajectory of the ball between the maximum height and the moment of impact can be described by

$$z_b^i[i] = z_b^m[i] - \frac{g}{8}(\Delta t)^2. \tag{5.10}$$

Solving this for Δt gives

$$\Delta t = \sqrt{\frac{8}{g}(z_b^m[i] - z_b^i[i])}. \tag{5.11}$$

Derivation of measurement Δp

Finally, an expression for the measurement of Δp is obtained. The basis of this is the conservation of momentum

$$v_b^o[i+1] = \frac{\Delta p}{m_b} + v_b^i[i]. \tag{5.12}$$

$v_b^o[i+1]$ can be replaced by using Equation (5.7), from which it can be found that

$$(1+e)v_p - ev_b^i[i] = \frac{\Delta p}{m_b} + v_b^i[i]. \tag{5.13}$$

The velocity $v_b^i[i]$ can be replaced by the conversion of kinetic energy to potential energy. Rewriting to an expression for Δp results in

$$\Delta p = m_b \left((1+e)v_p + (1+e)\sqrt{2g(z_b^m[i] - z_b^i[i])} \right). \tag{5.14}$$

5.4.3 Conclusion

A disadvantage of this method is that the functions f and h are reliant on the COR. It has been concluded before, in Section 3.2.1, that the COR varies for each bounce and is difficult to obtain correctly. For simplification of the functions, it is assumed that the COR has a known, constant value.

In summary, the analytical relations for the prediction and measurements can be written as

$$z_b^m[i+1] = \frac{\left((1+e)v_p + e\sqrt{2g(z_b^m[i] - z_b^i[i])} \right)^2}{2g} + z_b^o[i+1] + n_f \tag{5.15}$$

$$\Delta t = \sqrt{\frac{8}{g}(z_b^m[i] - z_b^i[i])} + n_g \tag{5.16}$$

$$\Delta p = m_b \left((1+e)v_p + (1+e)\sqrt{2g(z_b^m[i] - z_b^i[i])} \right) + n_h. \tag{5.17}$$

5.5 Emperical results

To verify the contact force estimation during bouncing and the parametrisation as established in the previous section, experiments have been done on the T-Flex. In this section, the set-up and method are presented. This is followed by the results of the tests with and without moving platform and a brief discussion of those.

5.5.1 Set-up

For the tests, only vertical bouncing has been done. To constrain the ball, an acrylic tube with an inner diameter of 80 mm and a length of 1 m is used. The tube is tight-fitted into a 3D-printed flange, which is mounted in the middle of the end-effector of the T-Flex, see Figure 5.6. Multiple holes are drilled at the bottom of the tube, right above the flange, to let the air out when the ball is falling. At 0.22 m, 0.47 m, 0.72 m and 0.97 m, holes are drilled to insert a pin. The pin can be pulled out, to release the ball from any of those heights. The locations of the holes are chosen such, that the centre of the ball is at 0.25 m, 0.5 m, 0.75 m and 1 m. At the bottom, a steel plate is placed, to make sure that the ball bounces on an even surface.

5.5.2 Method

Two types of tests were done, one where the end-effector was held at its neutral position, and one where the end-effector was moving at different velocities.

Since the tube is mounted onto the end-effector but not included in the mass matrix of the inverse dynamics of the T-Flex, it will be estimated as a contact force. This is compensated for by subtracting the force due to the gravity and acceleration of the tube and flange. For the experimental validation, the contact force on an empty platform is not necessarily zero. This might for example be due to the offset as discussed in Section 5.2. Therefore, the force threshold

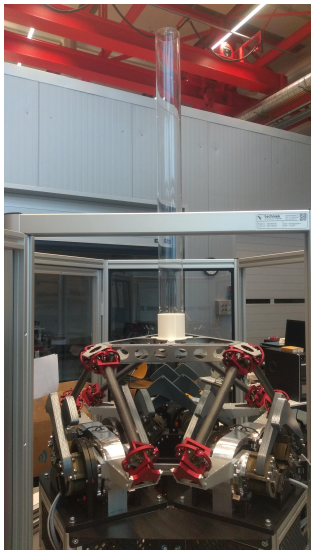

(a) The T-Flex with the tube.

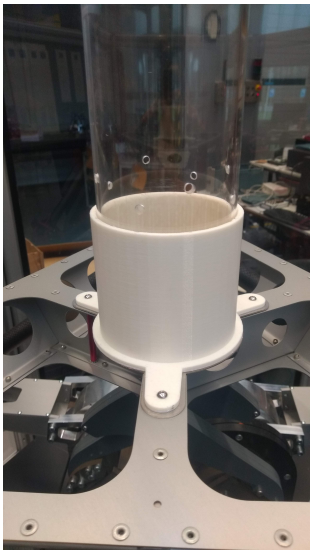

(b) Detail of the flange on the end-effector.

Figure 5.6: The test set-up. An acrylic tube is mounted on the T-Flex, using a 3D-printed flange.

is set at 5 N. The impact already starts before the contact force exceeds the threshold, however. Taking $t^i[i]$ and $t^o[i+1]$ as the moments that the contact force crosses the threshold, would mean that $\Delta p[i]$ would be lower than the actual impulse. To account for this, five samples are added to the start and end of the impact. From some testing, this seems sufficient to capture the whole impact. Additionally, the contact force that is not zero when there is no impact, also means that the measured contact force is higher than it actually is. This will result in a value for Δp that is too high. This is prevented by taking the mean of 40 samples before the impact and subtracting this from the measured contact force.

A camera is placed roughly 25 cm above the end-effector and at approximately 1 m from the tube. The bounces are filmed at a frame rate of 60 fps. The camera footage is analysed using the Matlab Image Processing Toolbox, with the method described in [53]. The height of the flange is taken as a reference, as this is a known distance. The distance between the end-effector and both the top and bottom of the ball is measured, from which the distance between the end-effector and the centre of the ball can be found. This is the ball height in the local end-effector frame. The camera measurements are taken as ground truth for the ball height. The measurements for Δt and Δp are obtained as described in Section 3.4, where t^i and t^o are the moments at which the contact force crosses the threshold, plus or minus five samples, respectively. The height of the ball is calculated as in Equation (5.9), with a fixed COR of 0.75.

After several bounces, the bounces follow quickly after each other, with lower contact force. This might result in the calculation of Δt and Δp taking into account multiple consecutive bounces, giving a larger value than expected. Therefore, it is checked whether a calculation of Δp resulted in a higher value than the preceding bounces and if so, all data from that bounce and the succeeding ones are discarded.

5.5.3 Tests without moving platform

For the tests without moving end-effector, the ball was dropped from each height three times. The camera measurement of the ball height can also be used to calculate a ground truth value

for Δt and Δp. For Δt this is

$$\Delta t = \sqrt{\frac{8}{g}(z_b^m[i])} \tag{5.18}$$

where $z_b^m[i]$ is the height of the ball in local frame. The ground truth for Δp can be calculated from the conservation of momentum, using

$$\begin{aligned} \Delta p &= m_b(v_b^o[i+1] - v_b^i[i]) \\ \Delta p &= m_b(\sqrt{2gz_b^m[i+1]} + \sqrt{2gz_b^m[i]}) \\ \Delta p &= m_b\sqrt{2g}(\sqrt{z_b^m[i+1]} + \sqrt{z_b^m[i]}). \end{aligned} \tag{5.19}$$

Since $v_p = 0$, the relations for $z_b^m[i+1]$, Δt and Δp only are dependent on $z_b^m[i]$. In Figure 5.7, the ground truth values of these parameters are shown in red. In yellow, the calculated values are shown. The blue curve is the analytical expression for each parameter.

It can be observed in the plot with results for Δt, that there is no data for bounces higher than 0.25 m. Since there is no value for Δt is available with the first bounce and the COR is lower for higher bounces, the second bounce has drastically decreased in height. Therefore data about Δt is only available in the lower range.

Another observation is that for bounces higher than approximately 0.25 m, the ground truth measurements deviate from the analytical relations. In these analytical relations, air resistance is neglected. However, with higher bounce heights, and thus higher ball velocities, air resistance is not negligible, as it is quadratically related to the velocity.

Because of the lack of measurements and the influence of air resistance, it is decided to limit the analysis only to the bounces below 0.25 m. The data in this range is shown in Figure 5.8.

It is seen that the model for $z_b^m[i+1]$ and Δt show good performance compared to the ground truth and the analytical relation. However, the measurements for Δp appear too low. In Figure 5.9, the measured impulse and the impulse from the ground truth are plotted against each other. On average, the impulse is estimated 31 % too low, when compared to the ground truth of Δp. It is yet unknown why this is the case.

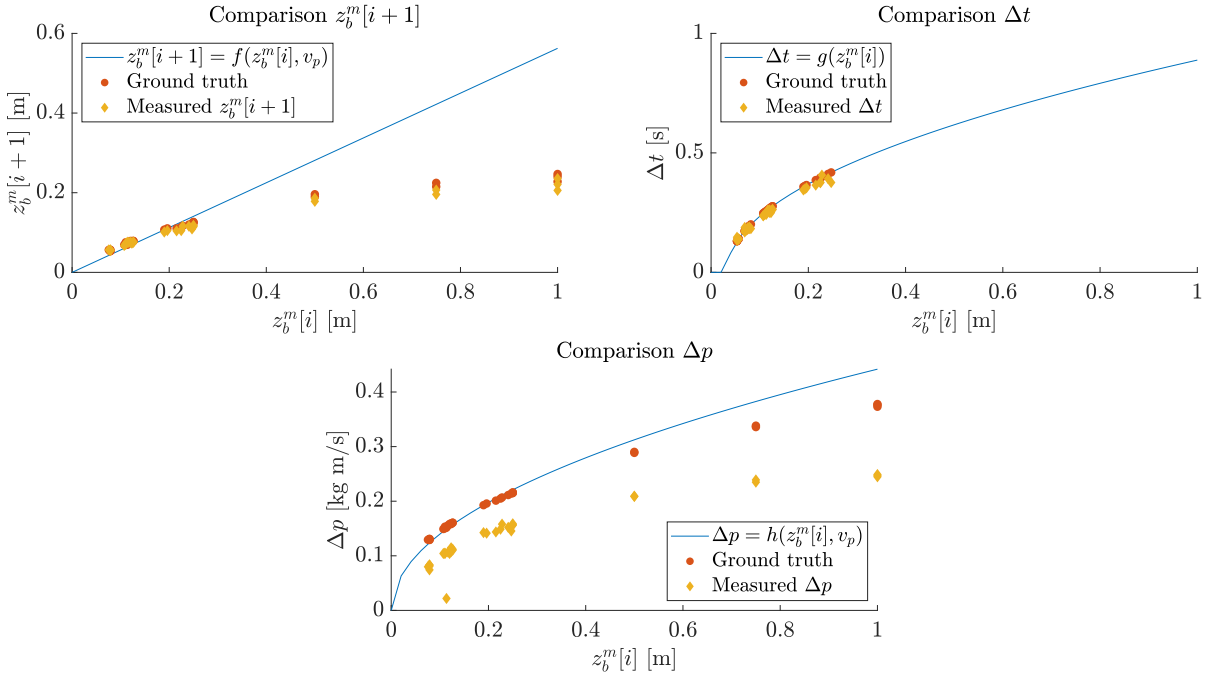

Figure 5.7: Estimation of $z_b^m[i+1]$, Δt and Δp compared to the ground truth measurement and analytical relation, with $e = 0.75$.

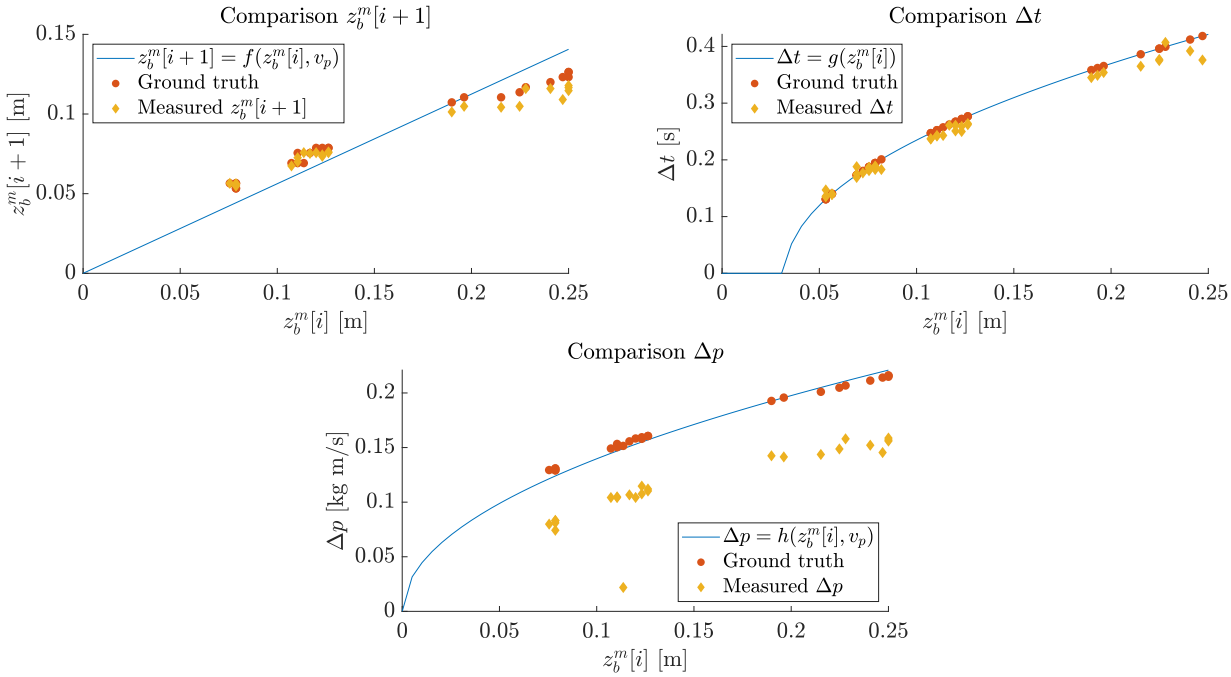

Figure 5.8: Estimation of $z_b^m[i+1]$, Δt and Δp compared to the ground truth measurement and analytical relation, with $e = 0.75$. Only data from bounces up to 0.25 m is considered.

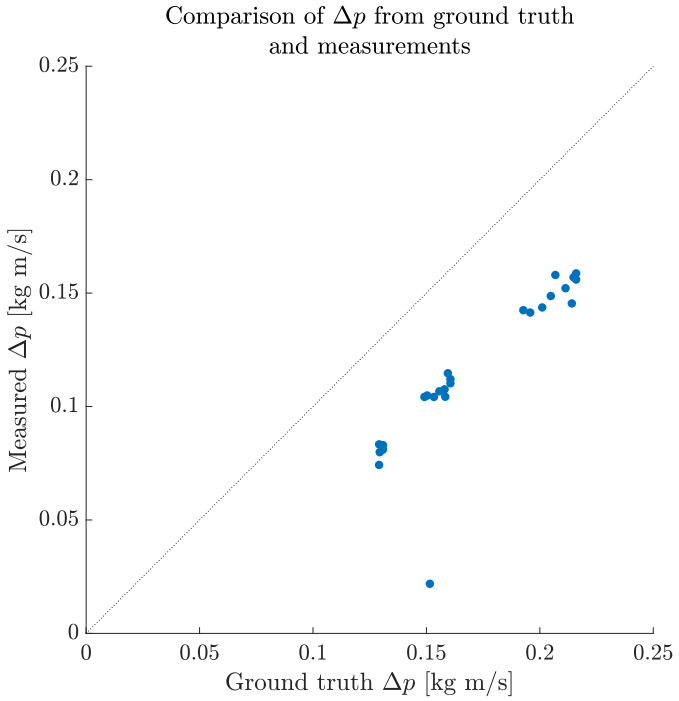

Figure 5.9: A comparison of the measured and ground truth Δp.

5.5.4 Tests with moving platform

For the tests with a moving platform, a sine reference profile is used for the end-effector. The used sines have an amplitude of 0.04 m and the frequency is varied. For each frequency, the test is repeated three times. The ball is dropped from 1 m above the end-effector. These tests are not recorded with a camera, so there are no ground truth measurements.

For $z_b^m[i+1]$ and Δp, a surface plot can be made, with $z_b^m[i]$ and v_p on the horizontal axes, and either of the parameters on the vertical axis. The platform velocity at the start of the impact is recorded. These surface plots and the measurements are shown in Figure 5.10 and Figure 5.12, respectively. For Δt, the measurements and analytical relation are shown in Figure 5.11. This is not a surface plot but a curve, since the expression for Δt is not dependent on v_p. Again, only the measurements of bounces below 0.25 m are shown.

In general, the same observations can be done as for the experiments without moving end-effector. The estimations for the ball height follow the surface well. It can also be observed that the measured Δt are around the curve, but not necessarily on it, as was the case with the experiments without moving end-effector. In the derivation of the expression for Δt, it was assumed that the maximum height of the ball is obtained at $\frac{1}{2}\Delta t$, but this is not necessarily true when the end-effector has a velocity.

For Δp, there is no clear offset, as could be observed in Figure 5.9. However, there is a large distribution of measurements and the majority is lower than expected based on the relation for Δp.

Although the mass of the tube is compensated for in the contact force estimation, the effect of the tube is still present in the parameter estimation. The tube is only fastened at the bottom

and does sway due to its length. This introduces additional inertia that is not accounted for in the inverse dynamics model.

Accuracy of Δt estimation

The standard deviation of the estimation error for Δt is relevant for the trajectory of the end-effector: the duration of the constant velocity is equal to twice this standard deviation. The standard deviation can be found by comparing the estimate of Δt with the measured Δt. First, $z_b^m[i+1]$ is calculated by Equation (5.9), using either the ground truth measurements in the case the platform was not moving or the measured value for $z_b^m[i+1]$ in the experiments with moving platform. Using this, Δt can be found following Equation (5.11). The comparison of the predicted values for Δt and the measured values is shown in Figure 5.13 The standard deviation can now be calculated for the error between this estimate and the measured value for Δt. The value of the standard deviation σ is 0.0501 s.

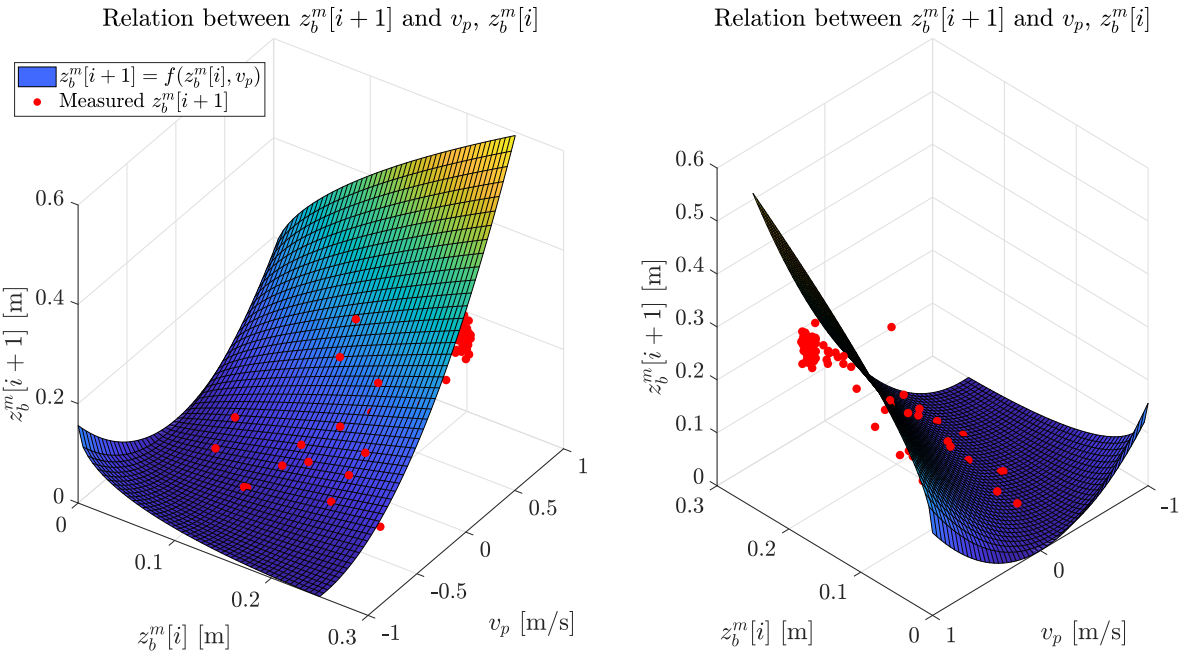

Figure 5.10: Estimations for $z_b^m[i+1]$, indicated with the red dots, for a moving end-effector and $e = 0.75$. The analytical relation is shown as the surface. The same graph is shown from two sides.

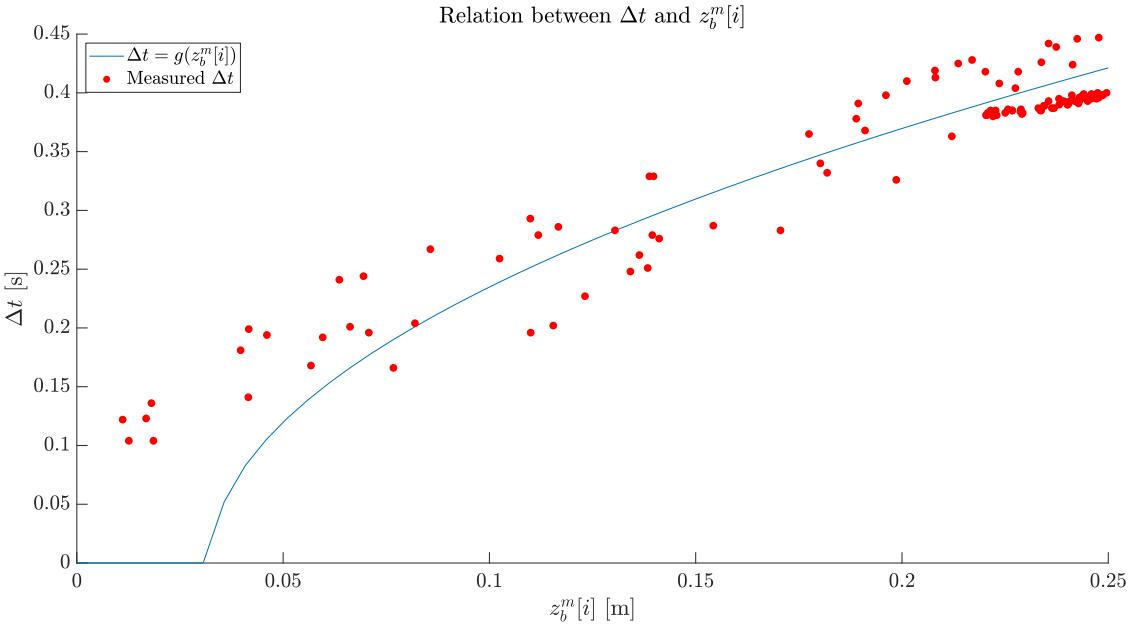

Figure 5.11: Measurements for Δt indicated with the red dots, for the moving end-effector. The analytical relation is shown as the blue curve.

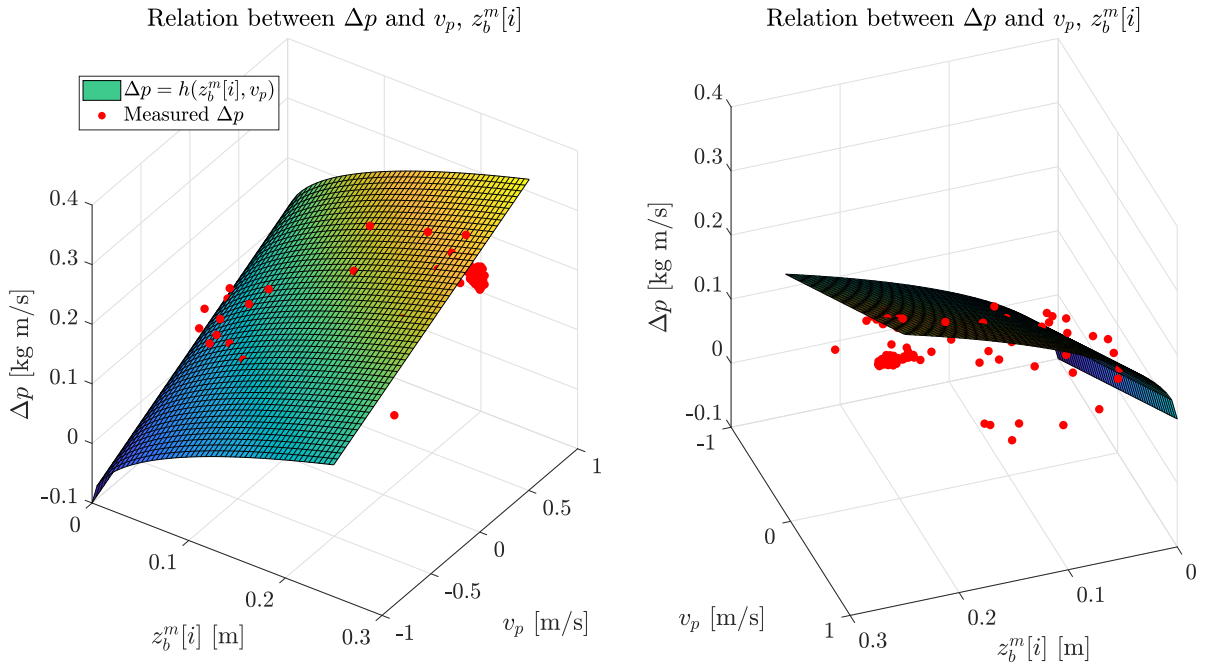

Figure 5.12: Estimations for Δp, indicated with the red dots, for a moving end-effector and $e = 0.75$. The analytical relation is shown as the surface. The same graph is shown from two sides.

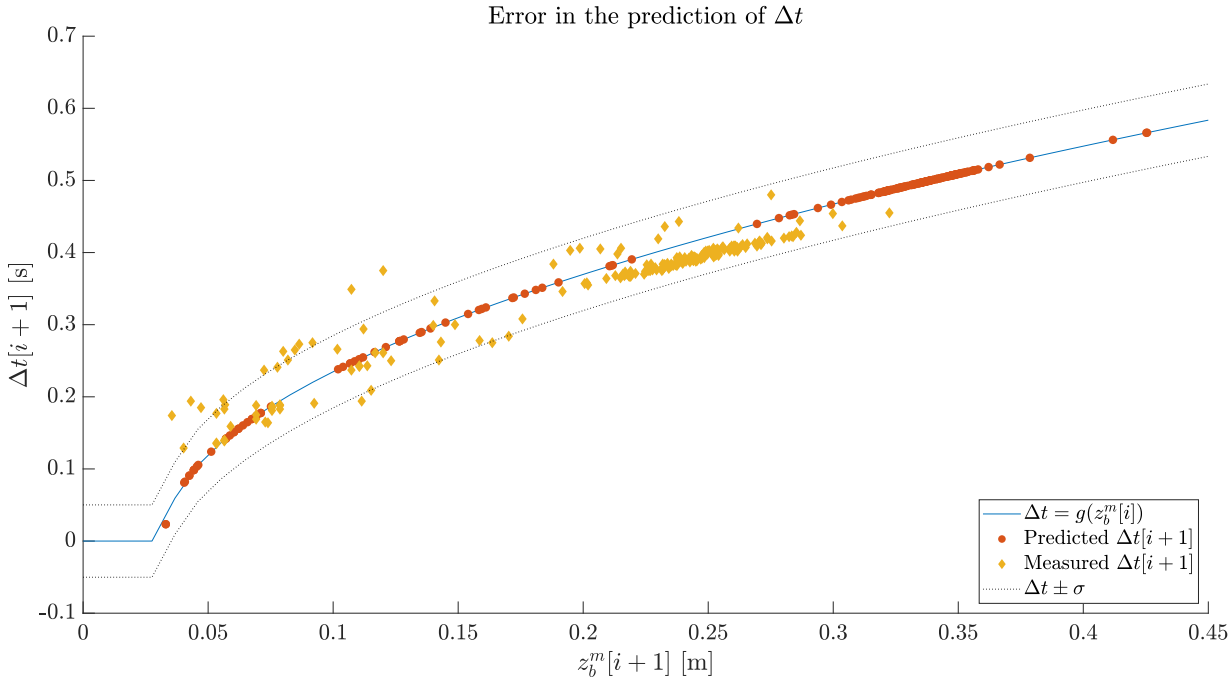

Figure 5.13: Prediction for the value of $\Delta t[i+1]$, based on the measurement of the ball height of the previous bounce and the platform velocity, in red dots. The prediction is compared to the measured value for $\Delta t[i+1]$, in yellow diamonds. The found standard deviation is shown in dotted lines.

5.6 Feasibility

From the experiments, it is found that the estimation of the linear impulse is inaccurate. Therefore, no working demonstration is available yet. To show the feasibility of bouncing a ball with the T-Flex, four scenarios are analysed.

The feasibility of bouncing a ball depends on multiple factors, for example, the allowed maximum acceleration of the platform, its travel range, the type of ball and the estimation errors in the parameters. To limit the feasibility analysis, the one-dimensional bouncing case is considered where a ball with COR = 0.75 is dropped from two different heights. Additionally, two different durations of the trajectory are considered.

The assessment of the feasibility of bouncing with the T-Flex is twofold. The available workspace needs to be large enough to accommodate the constant velocity over an interval of 2σ and the time it takes to finish the prescribed trajectory needs to be shorter than the available time. A position reference for the end-effector with relevant times and distances indicated, is shown in Figure 5.14.

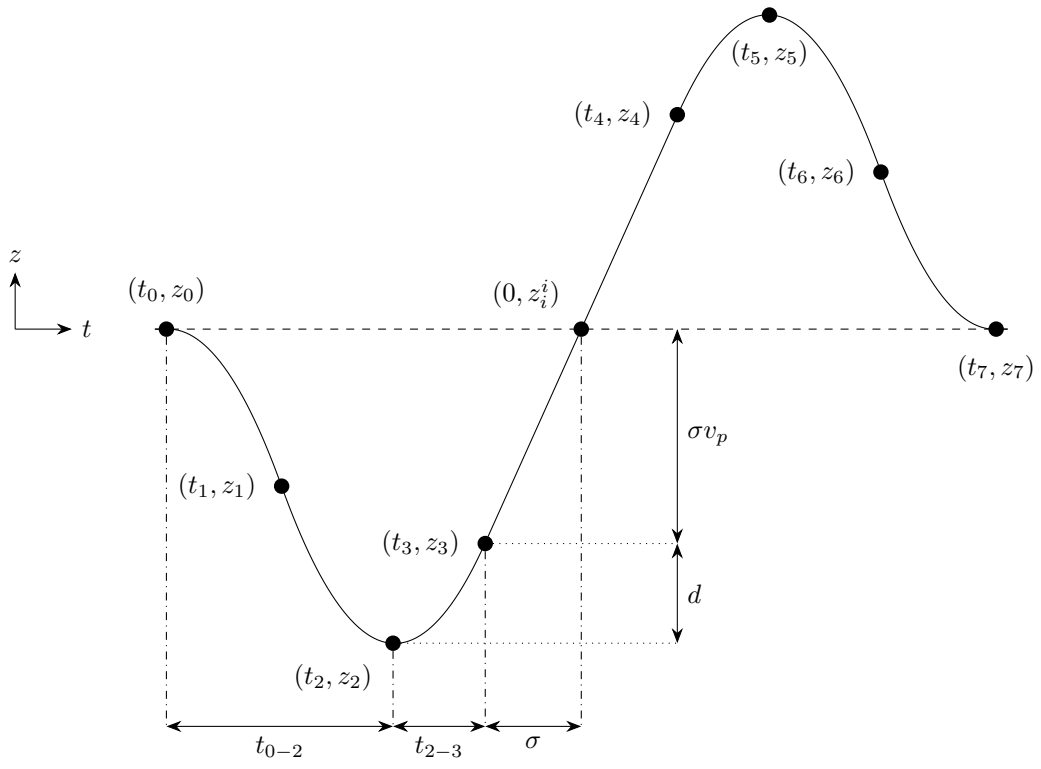

Figure 5.14: Trajectory of the end-effector in z-direction, with the times and distances that are relevant for the feasibility analysis.

5.6.1 Allowed workspace

From the empirical results described in Section 5.5, it was found that $\sigma = 0.0501$ s. First, the situation with drop height $z_b^m[i-1] = 0.2$ m and reference height $z_{ref} = 0.2$ m is considered. The maximum platform acceleration is assumed to be $a_{p,z} = g$. It can be calculated from

Equation (3.15) that the platform velocity $v_{p,z}$ to achieve this bounce should be 0.283 m/s. From this, it is possible to calculate the lowest position of the T-Flex during this trajectory. This can be found by adding the distances $\sigma v_{p,z}$, half of the distance covered during the constant velocity, and d, the distance during the acceleration from $v_{p,z} = 0$ m/s to $v_{p,z} = 0.283$ m/s. The lowest position is therefore

$$z_2 = -(\sigma v_{p,z} + d) = -(\sigma v_{p,z} + \frac{v_{p,z}^2}{2a_{p,z}}) = -0.0183\,\text{m} \tag{5.20}$$

The individual range of the T-Flex in z-direction is ±0.1 m [1], so this is within the workspace limits.

5.6.2 Required time for the trajectory

The second consideration for feasibility is the time that is needed to move the platform while the ball is in the air. The time between two bounces with the given reference height can be calculated using the outgoing velocity

$$v_{b,z}^o = \sqrt{2gz_{ref}} = 1.98\,\text{m/s}, \tag{5.21}$$

which results in

$$\Delta t = \frac{2v_{b,z}^o}{g} = 0.404\,\text{s}. \tag{5.22}$$

To assess whether this is sufficient to let the end-effector do an entire trajectory between two bounces, it is calculated how long this takes. Since the trajectory is symmetric, it suffices to look at half a trajectory. This consists of three parts: from the start (t_0) to the lowest position (t_2), from the lowest position to the start of the constant velocity (t_3) and the constant velocity until time of impact (t^i).

1. The time it takes to move from t_0 to t_2 is

$$t_{0-2} = 2\sqrt{\frac{z_2}{a_{p,z}}} = 0.0863\,\text{s}. \tag{5.23}$$

2. The time it takes to accelerate from $v_{p,z} = 0$ m/s at t_2 to $v_{p,z} = 0.283$ m/s at t_3 is found as

$$t_{2-3} = \frac{v_{p,z}}{a_{p,z}} = 0.0288\,\text{s}. \tag{5.24}$$

3. Half of the constant velocity interval takes $\sigma = 0.0501$ s.

Therefore, in total, half of the trajectory takes 0.1652 s to complete. After the impact of the ball, the second half of the trajectory needs to be completed, and the first half of the subsequent trajectory needs to be executed, to accommodate for the next bounce. Under the assumption that the ball impacts the end-effector exactly at time t_i, this takes 0.3305 s.

5.6.3 Extension to longer constant velocity

The previously calculated feasibility used a duration of the constant velocity of 2σ, which accounts for approximately 68% of the bounces. When this interval is elongated to 4σ, approximately 95% of the bounces are correctly intercepted. This has consequences for both the depth of the trajectory and the required time. The lowest position of the trajectory can be found from

$$z_2 = -(2\sigma v_{p,z} + d) = -(2\sigma v_{p,z} + \frac{v_{p,z}^2}{2a_{p,z}}) = -0.0324\,\text{m} \tag{5.25}$$

This is within the workspace limits of the T-Flex. The required time can be recalculated as well, where only the time for the constant velocity changes. This results in a total time of the half trajectory of 0.2057 s, so 0.4113 s for the full trajectory. This is longer than the time between two bounces. However, the needed time can be decreased by a higher maximum acceleration and/or using a ball with a higher COR. By choosing a ball with a higher COR, a lower platform velocity is required to bounce to the same reference height. This decreases the stroke of the end-effector and the time needed to accelerate.

5.6.4 Higher bouncing height

Additionally, it has been checked whether bouncing is feasible for higher bouncing heights. Both $z_b^m[i-1]$ and z_{ref} are now set to 0.5 m. The COR is still 0.75. The time between two bounces would now be 0.6386 s. For the case with a constant velocity duration of 2σ, the lowest point of the trajectory would be at -0.033 m. The total time for the trajectory is 0.422 s. This is feasible. In the situation with a constant velocity duration of 4σ, the lowest point is at -0.055 m and the total required time is 0.5912 s. This is feasible as well.

5.6.5 Conclusion

The feasibility of ball bouncing with the T-Flex has been evaluated for two reference heights and two durations of the trajectory. For both bouncing heights, the needed time to complete the trajectory is within the available time for a constant velocity duration of 2σ. However, for the trajectory with a constant velocity duration of 4σ, bouncing is not feasible for lower bouncing heights. It should be noted that the assumed acceleration in z-direction is lower than the limit of the T-Flex and the COR could be increased by using a different ball. Therefore, bouncing a ball using the T-Flex with the given conditions is deemed feasible.

Chapter 6

Conclusion

To showcase the properties of the T-Flex, a bouncing ball demonstration is found to be most suitable, based on a comparison of existing demonstrations and several criteria. It shows three out of four features of the T-Flex, it requires a low amount of preparation and supervision and has a high degree of attractiveness. However, the repeatability is not shown in this demonstration, although this is one of the main features of the T-Flex.

A description for a one-dimensional bouncing ball is developed, where use is made of the possibility to measure the contact force on the T-Flex end-effector. The linear impulse and time between consecutive bounces can be found using these contact forces, from which the ball velocities can be calculated. Based on the ball velocities, the required platform velocity is found, which is the control variable for the ball height. This bouncing algorithm is verified in simulations.

The simulations show that the relative error for the parameter estimation for the ball velocities, prediction of the incoming velocity and impact time is between -15% and +5 % approximately. For the estimation of the incoming ball velocity, this is between approximately -8% and +2 %. Active bouncing is feasible in simulation, given that the difference between the drop height of the ball and the reference bouncing height is not too large. However, the reference height is achieved less accurately with higher contact damping and a higher reference height.

The one-dimensional model is expanded to two-dimensions, where the ball is bouncing sideways. The parameters that need to be controlled are the ball velocity in x- and z-direction and the angle of departure. A simulation is done as a proof of concept, which shows that additional work is required to make the two-dimensional bouncing functional. The simulation is not robust for different combinations of parameters and an intermediate bounce can be seen, possibly due to errornous estimations of $\hat{x}_b^i[i+1]$ and $\hat{v}_{b,x}^i[i+1]$.

For the experiments of one-dimensional ball bouncing on the T-Flex, an alternative description for the ball trajectory is developed, to better investigate the inaccuracies in the measurements and parameter estimation. From experiments, it was found that the linear impulse is estimated approximately 31% too low on a non-moving platform. For the experiments with moving platform, this was too low as well, although with larger distribution. Additionally, the assumption that air resistance is negligible is found to only hold up to 0.25 m, making the found analytical relations inaccurate for higher bouncing heights. The standard deviation of the estimation error for Δt is approximately 0.05 s, which is of large influence on the duration of the platform trajectory.

Finally, the feasibility of bouncing with the T-Flex has been demonstrated. For a bouncing height of 0.2 m, it is found that bouncing is indeed feasible for the stroke and acceleration capabilities of the T-Flex.

Chapter 7

Recommendations

A start is made with the development of a ball bouncing demonstration for the T-Flex and although the demonstration is not fully functional yet, it is recommended to continue its development. This is supported by the high scoring in the demonstration selection and the results of the feasibility analysis.

To obtain a working demonstration, it is advisable to investigate the estimation for the linear impulse on the T-Flex. From the experimental results, it is found that the estimation is too low. Additionally, only bounces up to 0.25 m are considered, as the derived parameter estimation becomes inaccurate above this height due to neglected air resistance. For higher bouncing, the air resistance is considerable and it is therefore advisable to include air resistance in the trajectory model. During experiments with a moving end-effector, it is observed that the tube, that is used to constrain the ball, sways. This introduces unmodelled inertia terms, resulting in an inaccurate contact force estimation. To improve the estimation, it would be advisable to either do the identification of the parameters for the inverse dynamics including the tube, or mount the tube above the end-effector, such that the inverse dynamics are not affected. Additionally, it has been observed that a tennis ball does damp out quickly. Switching to a different ball with a higher COR might be beneficial.

In this work, two different ball trajectory parameterisations are established, one using the ball velocity and the other using the bounce height. It is recommended to use the former method, given that the measurement of the linear impulse is correct. In the latter method, the relations for the ball bounce height and the measurement Δp are functions of the COR. Since the COR is unknown beforehand, this method would be more unreliable than the parameter estimation with velocity, which only relies on measurements and physical relations.

The demonstrator on the T-Flex can eventually be extended to two-dimensional or three-dimensional bouncing. To do so, the parameter estimation needs to be improved. From the simulation, it appears that two-dimensional bouncing is not robust for certain combinations of stiffness, damping, drop height and references. It is not clear whether this is due to modelling or implementation errors, or whether two-dimensional bouncing is indeed only feasible for a limited set of values. It would be advisable to investigate this, and how this would translate to bouncing on the T-Flex. Additionally, the cause of the intermediate bounces should be investigated as well, to achieve the sideways bouncing as intended.

Bibliography

[1] M. Naves, M. Nijenhuis, B. Seinhorst, W. B. J. Hakvoort, and D. M. Brouwer, "T-Flex: A fully flexure-based large range of motion precision hexapod," *Precision Engineering*, vol. 72, pp. 912–928, Nov. 2021. DOI: 10.1016/j.precisioneng.2021.08.015.

[2] R. M. Murray, Z. Li, and S. S. Sastry, *A Mathematical Introduction to Robotic Manipulation*. CRC Press, 1994, p. 132.

[3] M. Naves, R. G. K. M. Aarts, and D. M. Brouwer, "Large stroke high off-axis stiffness three degree of freedom spherical flexure joint," *Precision Engineering*, vol. 56, pp. 422–431, Mar. 2019. DOI: 10.1016/j.precisioneng.2019.01.011.

[4] M. Naves, M. Nijenhuis, W. B. J. Hakvoort, and D. M. Brouwer, "Flexure-based 60 degrees stroke actuator suspension for a high torque iron core motor," *Precision Engineering*, vol. 63, pp. 105–114, May 2020. DOI: 10.1016/j.precisioneng.2020.02.001.

[5] Precision Engineering, University of Twente. "T-Flex: Compliant Flexure-based Large Range Precision Hexapod," YouTube. (Aug. 22, 2022), [Online]. Available: https://www.youtube.com/watch?v=tenxq7N5q3k.

[6] ABB Robotics. "ABB Robotics - Fanta Can Challenge- Level II - Superior Motion Control," YouTube. (Oct. 12, 2009), [Online]. Available: https://www.youtube.com/watch?v=SOESSCXGhFo.

[7] Reach Lab at UTK. "Parallel Continuum Manipulator Demo," YouTube. (Jun. 8, 2014), [Online]. Available: https://www.youtube.com/watch?v=kdOPsmY6b24.

[8] Symetrie Hexapods. "SYMETRIE - ARROW: Accurate and Rapid Robots with a large Operational Workspace," YouTube. (Apr. 14, 2020), [Online]. Available: https://www.youtube.com/watch?v=a-oGrLi4xk8.

[9] SmarAct GmbH. "SmarPod Microassembling Demo," YouTube. (May 31, 2013), [Online]. Available: https://www.youtube.com/watch?v=5MSh1qcIOXk.

[10] MASTWORK. "Pentagon Robot, Five-bar robot Parallel SCARA linking to lead end-effector (SHOW1, side view)," YouTube. (Dec. 14, 2019), [Online]. Available: https://www.youtube.com/watch?v=_1XRtJ4bpl8.

[11] Full Motion Dynamics. "Ball and Plate PID control with 6 DOF Stewart platform," YouTube. (Dec. 14, 2019), [Online]. Available: https://www.youtube.com/watch?v=j4OmVLc_oDw.

[12] K. L. Poggensee, A. H. Li, D. Sotsaikich, *et al.*, "Ball juggling on the bipedal robot Cassie," Institute of Electrical and Electronics Engineers Inc., May 2020, pp. 875–880. DOI: 10.23919/ecc51009.2020.9143967.

[13] P. Reist and R. Drandrea, "Design and analysis of a blind juggling robot," *IEEE Transactions on Robotics*, vol. 28, pp. 1228–1243, 6 2012. DOI: 10.1109/TRO.2012.2205493.

[14] Physik Instrumente. "PI Hexapods for Fiber Alignment," YouTube. (Jan. 11, 2016), [Online]. Available: https://www.youtube.com/watch?v=V2Z_uyOrTtg.

[15] SmarAct GmbH. "PICOSCALE Interferometer Sensor Head Alignment Window," YouTube. (Jun. 29, 2020), [Online]. Available: https://www.youtube.com/watch?v=A6xMiCrpZdQ.

[16] MOTION FOR SIMULATORS /MFS. "Motion for simulators mfs 6DOF motion platform - REPEATABILITY DEMONSTRATION," YouTube. (Jul. 26, 2018), [Online]. Available: https://www.youtube.com/watch?v=WBxZ4LvIG0k.

[17] F. Ruggiero, V. Lippiello, and B. Siciliano, "Nonprehensile dynamic manipulation: A survey," *IEEE Robotics and Automation Letters*, vol. 3, no. 3, pp. 1711–1718, 2018. DOI: 10.1109/LRA.2018.2801939.

[18] T. Kizaki and A. Namiki, "Two ball juggling with high-speed hand-arm and high-speed vision system," Institute of Electrical and Electronics Engineers Inc., 2012, pp. 1372–1377. DOI: 10.1109/ICRA.2012.6225090.

[19] T. Hsiao and S. C. Wu, "Decision making based on physical and neural network models for precision ball-batting robots," vol. 2021-May, Institute of Electrical and Electronics Engineers Inc., May 2021, pp. 3787–3792. DOI: 10.23919/ACC50511.2021.9482718.

[20] H. Li, H. Wu, L. Lou, K. Kühnlenz, and O. Ravn, "Ping-pong robotics with high-speed vision system," 2012, pp. 106–111. DOI: 10.1109/ICARCV.2012.6485142.

[21] Z. Zhang, D. Xu, and M. Tan, "Visual measurement and prediction of ball trajectory for table tennis robot," *IEEE Transactions on Instrumentation and Measurement*, vol. 59, pp. 3195–3205, 12 Dec. 2010. DOI: 10.1109/TIM.2010.2047128.

[22] A. Nakashima, Y. Sugiyama, and Y. Hayakawa, "Paddle juggling of one ball by robot manipulator with visual servo," 2006. DOI: 10.1109/ICARCV.2006.345164.

[23] M. Bühler, D. E. Koditschek, and P. J. Kindlmann, "A simple juggling robot: Theory and experimentation," in *Experimental Robotics I*, V. Hayward and O. Khatib, Eds., Berlin, Heidelberg: Springer Berlin Heidelberg, 1990, pp. 35–73.

[24] A. Pekarovskiy, K. Saluja, R. Sarkar, and M. Buss, "Resonance-driven dynamic manipulation: Dribbling and juggling with elastic beam," Institute of Electrical and Electronics Engineers Inc., Sep. 2014, pp. 943–948. DOI: 10.1109/ICRA.2014.6906967.

[25] R. Ronsse, P. Lefèvre, and R. Sepulchre, "Sensorless stabilization of bounce juggling," *Robotics, IEEE Transactions on*, vol. 22, pp. 147–159, Mar. 2006. DOI: 10.1109/TRO.2005.858860.

[26] R. Ronsse and R. Sepulchre, "Feedback control of impact dynamics: The bouncing ball revisited," Institute of Electrical and Electronics Engineers Inc., 2006, pp. 4807–4812. DOI: 10.1109/cdc.2006.376774.

[27] L. Kiltz, M. Janocha, and J. Rudolph, "Algebraic estimation of impact times: Juggling a ball with a magnetically levitated plate," 2013, pp. 145–149. DOI: 10.1109/IcConSCS.2013.6632038.

[28] Z. Shareef, V. Just, H. Teichrieb, and A. Trächtler, "Design and control of cooperative ball juggling delta robots without visual guidance," *Robotica*, vol. 35, pp. 384–400, 2 Feb. 2017. DOI: 10.1017/S0263574715000569.

[29] G. Bätz, K. K. Lee, D. Wollherr, and M. Buss, "Robot basketball: A comparison of ball dribbling with visual and force/torque feedback," Institute of Electrical and Electronics Engineers Inc., 2009, pp. 514–519. DOI: 10.1109/ROBOT.2009.5152413.

[30] H. Zhao, S. Wang, G. Zhou, and W. Jung, "Tenniseye: Tennis ball speed estimation using a racket-mounted motion sensor," Association for Computing Machinery, Inc, Apr. 2019, pp. 241–252. DOI: 10.1145/3302506.3310404.

[31] P. Blank, B. H. Groh, and B. M. Eskofier, "Ball speed and spin estimation in table tennis using a racket-mounted inertial sensor," vol. Part F130534, Association for Computing Machinery, Sep. 2017, pp. 2–9. DOI: 10.1145/3123021.3123040.

[32] Physik Instrumente. "High-Dynamics and High-Precision Laser Processing for Wafer Dicing," YouTube. (Jan. 26, 2020), [Online]. Available: https://www.youtube.com/watch?v=k8owq_ouvOA.

[33] TPREX. "Delta robot pick and place demonstration," YouTube. (Apr. 6, 2014), [Online]. Available: https://www.youtube.com/watch?v=TWSf8OC8Qu0.

[34] Nathan. "Ball Balancing PID System," YouTube. (Oct. 3, 2014), [Online]. Available: https://www.youtube.com/watch?v=7Jw8m4pbTYI.

[35] T. Glück, A. Eder, and A. Kugi, "Swing-up control of a triple pendulum on a cart with experimental validation," *Automatica*, vol. 49, pp. 801–808, 3 Mar. 2013. DOI: 10.1016/j.automatica.2012.12.006.

[36] A. Zeng, S. Song, J. Lee, A. Rodriguez, and T. Funkhouser, "Tossingbot: Learning to throw arbitrary objects with residual physics," Mar. 2019. DOI: 10.48550/arxiv.1903.11239.

[37] Stuff Made Here. "I made a 100mph flying hoop," YouTube. (Jun. 6, 2022), [Online]. Available: https://www.youtube.com/watch?v=xHWXZyfhQas.

[38] B. Bäuml, T. Wimböck, and G. Hirzinger, "Kinematically optimal catching a flying ball with a hand-arm-system," 2010, pp. 2592–2599. DOI: 10.1109/IROS.2010.5651175.

[39] P. Reist and R. D'Andrea, "Control of nonlinear systems with symmetries using chaos," Institute of Electrical and Electronics Engineers Inc., 2012, pp. 997–1002. DOI: 10.1109/CDC.2012.6426220.

[40] P. Reist and R. D'Andrea, "Design of the pendulum juggler," 2011, pp. 5154–5159. DOI: 10.1109/ICRA.2011.5979789.

[41] D. Brescianini, M. Hehn, and R. D'Andrea, "Quadrocopter pole acrobatics," 2013, pp. 3472–3479. DOI: 10.1109/IROS.2013.6696851.

[42] CrudenSimulators. "Cruden B306-HMD motorcycle simulator - first footage," YouTube. (May 19, 2017), [Online]. Available: https://www.youtube.com/watch?v=DHQYniah_GM.

[43] Martin Laubner. "Cessna 172 Full Motion Flight Simulator - Thunderstorm Flying!" YouTube. (Jun. 18, 2016), [Online]. Available: https://www.youtube.com/watch?v=4KhMmSEoxMs.

[44] SmarAct GmbH. "SMARPOD - A Hexapod-like Positioning System." (2022), [Online]. Available: https://www.smaract.com/en/smarpod (visited on 12/23/2022).

[45] Tobias Glück. "Triple Pendulum on a Cart," YouTube. (Mar. 29, 2011), [Online]. Available: https://www.youtube.com/watch?v=cyN-CRNrb3E.

[46] Zeeshan Shareef. "Cooperative Ball Juggling Delta Robots without Visual Guidance," YouTube. (Mar. 20, 2015), [Online]. Available: https://www.youtube.com/watch?v=X0xvy4rViyE.

[47] J. L. Meriam, L. G. Kraige, and J. N. Bolton, *Engineering Mechanics: Dynamics*, 8th ed. Hoboken, NJ: Wiley, 2016, pp. 215, 216, SI Version.

[48] A. Haron and K. A. Ismail, "Coefficient of restitution of sports balls: A normal drop test," vol. 36, 2012. DOI: 10.1088/1757-899X/36/1/012038.

[49] R. Cross, "Coefficient of restitution for an obliquely bouncing ball," *Physics Education*, vol. 56, p. 015 004, 1 Nov. 2020. DOI: 10.1088/1361-6552/abbcbd.

[50] International Tennis Federation. "ITF approved tennis balls, classified surfaces & recognised courts 2022- a guide to products and test methods." (2022), [Online]. Available: https://www.itftennis.com/en/about-us/organisation/publications-and-resources/tennis-tech/ (visited on 12/02/2022).

[51] B. Seinhorst and W. Hakvoort, "Efficient formulation of hexapod kinematics enabling real time adaptive feedforward control," in *2021 IEEE/ASME International Conference on Advanced Intelligent Mechatronics (AIM)*, 2021, pp. 186–191. DOI: 10.1109/AIM46487.2021.9517402.

[52] S. Miller. "Simscape Multibody Contact Forces Library," GitHub. (2019), [Online]. Available: https://github.com/mathworks/Simscape-Multibody-Contact-Forces-Library/releases/tag/18.1.4.1 (visited on 12/08/2022).

[53] MathWorks. "Measure Distances in an Image." (), [Online]. Available: https://nl.mathworks.com/help/images/measure-distances-in-images.html (visited on 01/20/2023).

Appendix A

Rubric for scoring criteria of demonstration choice

Table A.1: The rubric for scoring each category of demonstrations for its suitability for the T-Flex. Each criterion is scored on a scale of one to five.

	1	**2**	**3**	**4**	**5**
Additional hardware	Multiple objects are needed and the setup needs to be modified.	Multiple objects are needed, and/or require some effort to be mounted.	One or multiple objects are needed, but are easily obtained and mounted.	An object is needed but is easily obtained, and does not need to be mounted.	Nothing is needed.
Preparation	The demonstration requires extensive knowledge to operate, the setup beforehand is complex.	Operating the demonstration requires extensive explanation beforehand, considerable time to setup beforehand.	Some explanation beforehand is necessary, setup time is moderate.	The demonstration needs to be explained shortly, and requires little setup.	No setup or explanation is needed before the demonstration,
Supervision	The demonstration needs to be closely attended continuously.	Supervision is often required, although not continuously.	The demonstration requires moderate supervision.	Little supervision is needed.	The demonstration can run without any supervision.
Adjust and extend	The demonstration is fixed, it cannot be adjusted or extended.	Some element of the demonstration can be adjusted or extended.	A limited set of adjustments and extensions can be done.	Multiple alterations and extensions are possible.	Can be completely altered and/or a lot of extensions are possible.
Originality and attractiveness	Not attractive and original at all, not captivating.	Does not capture much attention, no real original component.	Captures a bit of attention, has an original element.	Interesting and captivating, has multiple original elements.	Immediately catches the eye, very original.

Appendix B

Calculation of platform trajectory 1D bouncing

The desired trajectory for the end-effector consists of a linear part, with constant velocity v_p, and polynomials of second and third order. The ball is predicted to impact the end-effector at time t^i and the height of the platform at t_i is chosen to be the neutral position. At the time of impact, the platform should have the velocity v_p, to make sure that the ball bounces to the reference height. To account for prediction errors in t^i, there is an interval over which the platform moves with constant velocity. This interval has a width of 2σ, where σ is the standard deviation of the prediction error for t^i.

The interval of constant velocity starts at time

$$t_3 = t^i - \sigma \tag{B.1}$$

and ends at time

$$t_4 = t^i + \sigma. \tag{B.2}$$

With t_3 and t_4 known, the rest of the trajectory can be constructed as well. The trajectory is symmetric, the part of the trajectory between t^i and t_7 can be obtained by reversing and negating the trajectory between t_0 and t^i. Therefore, only the calculation of the first half of the trajectory will be shown.

The position of the platform at t^i is zero. The position of the platform at t_3 is then

$$z_3 = -\sigma v_p. \tag{B.3}$$

From t_2 to t_3 the platform undergoes a constant, maximum acceleration a_p. At t_2, the platform reaches the deepest position in the trajectory and has a velocity of zero. The time t_2 is found from

$$t_2 = t_3 - \frac{v_p}{a_p}. \tag{B.4}$$

Subsequently, the relation between positions z_2 and z_3 can be expressed as

$$z_2 = z_3 - \frac{1}{2} a_p (t_3 - t_2)^2. \tag{B.5}$$

The trajectory between t_0, the start of the trajectory, and t_2 can be divided into two parts of equal length: between t_0 and t_1 with maximum acceleration and between t_1 and t_2 with maximum deceleration. At time t_1, the maximum velocity v_{max} is achieved. The average velocity is denoted by v_{avg}.
The relation between the lowest point z_2 and the maximum velocity is

$$v_{max} = 2v_{avg} = \frac{2z_2}{t_2 - t_0}. \tag{B.6}$$

Additionally, since the platform starts with zero velocity, the maximum velocity can be expressed as

$$v_{max} = \frac{1}{2}(t_2 - t_0)a_p. \tag{B.7}$$

By substituting Equation (B.7) into Equation (B.6), the starting time of the trajectory t_0 can be found as

$$t_0 = t_2 - 2\sqrt{\frac{z_2}{a_p}} \tag{B.8}$$

and time t_1 as

$$t_1 = t_2 - \sqrt{\frac{z_2}{a_p}}. \tag{B.9}$$

Now z_1 can be calculated as

$$z_1 = \frac{1}{2}(t_1 - t_0)v_{max}. \tag{B.10}$$

The positions and times that have been calculated serve as boundary conditions for the polynomials that describe the trajectory. Between t_0 and t_1, a second order polynomial

$$z(t) = a_1 t^2 + a_2 t + a_3 \tag{B.11}$$

is used, with boundary conditions

$$v(t_0) = 0 \tag{B.12}$$
$$z(t_1) = z_1 \tag{B.13}$$
$$v(t_1) = v_{max}. \tag{B.14}$$

Solving for the coefficients results in

$$\begin{bmatrix} a_1 \\ a_2 \\ a_3 \end{bmatrix} = \begin{bmatrix} -v_{max}/(2(t_0 - t_1)) \\ (t_0 v_{max})/(t_0 - t_1) \\ (2t_0 z_1 - 2t_1 z_1 + t_1^2 v_{max} - 2t_0 t_1 v_{max})/(2(t_0 - t_1)) \end{bmatrix}. \tag{B.15}$$

Between t_1 and t_3, a third order polynomial

$$z(t) = b_1 t^3 + b_2 t^2 + b_3 t + b_4 \tag{B.16}$$

is used, as there are four boundary conditions, namely

$$z(t_1) = z_1 \tag{B.17}$$
$$v(t_1) = v_{max} \tag{B.18}$$
$$z(t_3) = z_3 \tag{B.19}$$
$$v(t_3) = v_p. \tag{B.20}$$

Solving for the coefficients results in

$$\begin{bmatrix} b_1 \\ b_2 \\ b_3 \\ b_4 \end{bmatrix} = \frac{1}{((t_1 - t_3)^3)} \begin{bmatrix} -(2z_1 - 2z_3 - t_1 v_{max} + t_3 v_{max} - t_1 v_p + t_3 v_p) \\ (3t_1 z_1 - 3t_1 z_3 + 3t_3 z_1 - 3t_3 z_3 - t_1^2 v_{max} + 2t_3^2 v_{max} - 2t_1^2 v_p + t_3^2 v_p - t_1 t_3 v_{max} + t1 t_3 v_p) \\ -(t_3^3 v_{max} - t_1^3 v_p + t_1 t_3^2 v_{max} - 2t_1^2 t_3 v_{max} + 2t_1 t_3^2 v_p - t_1^2 t_3 v_p + 6t_1 t_3 z_1 - 6t_1 t_3 z_3) \\ (t_1^3 z_3 - t_3^3 z_1 + t_1 t_3^3 v_{max} - t_1^3 t_3 v_p + 3t_1 t_3^2 z_1 - 3t_1^2 t_3 z_3 - t_1^2 t_3^2 v_{max} + t_1^2 t_3^2 v_p) \end{bmatrix}. \tag{B.21}$$

The third order polynomial does not give a constant acceleration, but the constraint on both the position and slope at t_1 and t_2 cannot be fulfilled with a second order polynomial.

The position during the constant velocity can be calculated by

$$z(t) = z(t - t_s) + v_p t_s, \tag{B.22}$$

where t_s is the sample time of the model.

Appendix C

Simulation model 1D bouncing

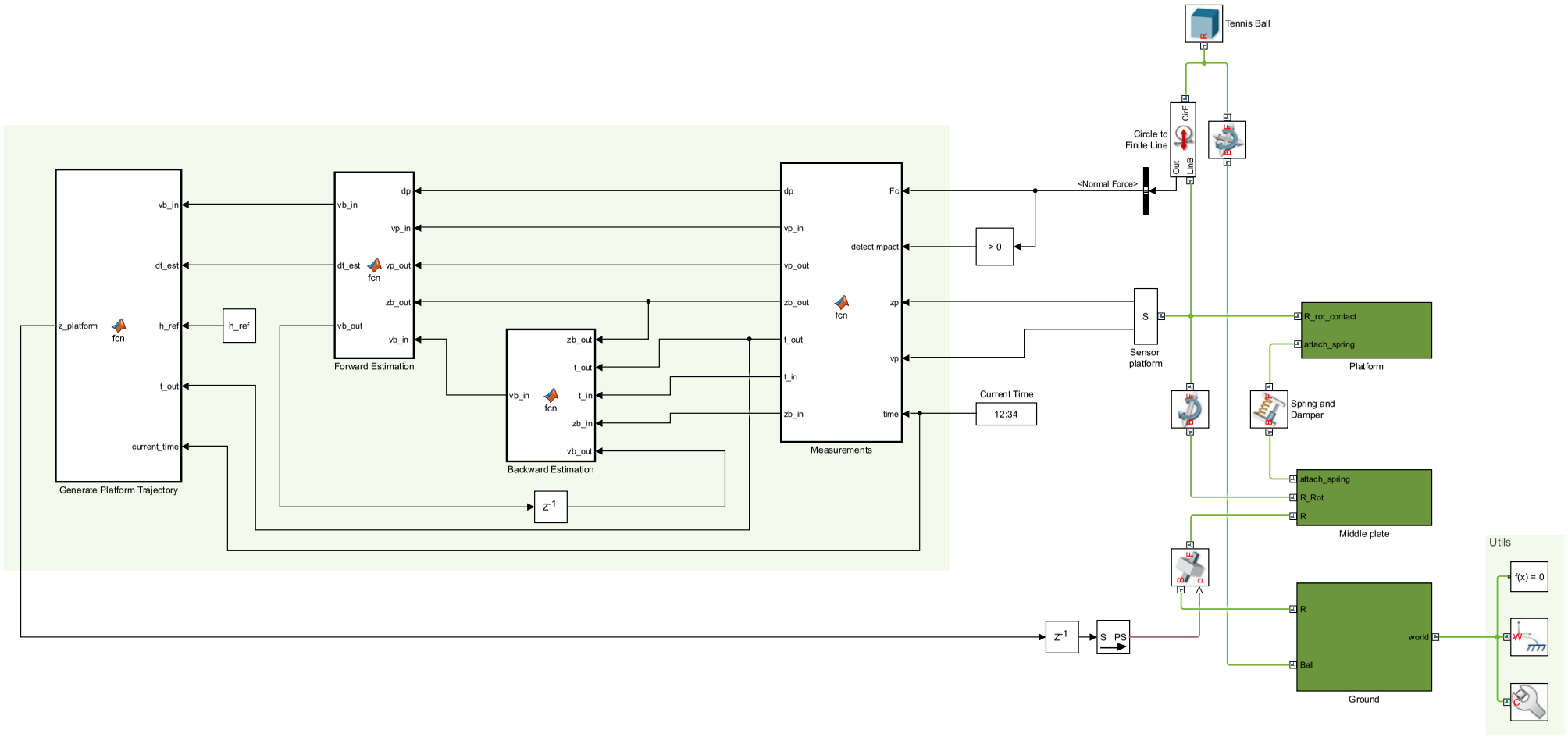
Tennis Ball
Circle to Finite Line
CirF
LinB
Out
<Normal Force>
> 0
Sensor platform
S
R_rot_contact
attach_spring
Platform
Spring and Damper
attach_spring
R_Rot
R
Middle plate
R
Ball
world
Ground
Utils
f(x) = 0
Measurements
dp
vp_in
vp_out
zb_out
t_out
t_in
zb_in
detectImpact
Fc
zp
vp
time
Forward Estimation
vb_in
dt_est
vp_out
zb_out
vb_out
dp
Backward Estimation
vb_in
zb_out
t_out
t_in
zb_in
vb_out
Generate Platform Trajectory
z_platform
h_ref
vb_in
dt_est
t_out
current_time
fcn
Current Time
12:34
S PS

Appendix D

Derivation of the angle of departure

The following derivation only concerns parameters of one single bounce. Therefore, the bounce index i is omitted for clarity. The maximum height of the ball is assumed to be achieved at time $\frac{1}{2}\Delta t$, therefore the maximum height of the ball can be expressed as

$$z_b^m = z_b^o + \frac{1}{2}v_{b,z}^o \Delta t - \frac{1}{8}g(\Delta t)^2. \tag{D.1}$$

The ball velocity $v_{b,z}^o$ can be written as a function of the absolute velocity and the angle of departure, resulting in

$$z_b^m = z_b^o + \frac{1}{2}\|\mathbf{v_b^o}\| \sin(\gamma)\Delta t - \frac{1}{8}g(\Delta t)^2. \tag{D.2}$$

The total horizontal distance that is covered by the ball trajectory can be expressed as

$$x_b^i = x_b^o + v_{b,x}^o \Delta t, \tag{D.3}$$

which can be rewritten as

$$x_b^i = x_b^o + \|\mathbf{v_b^o}\| \cos(\gamma)\Delta t. \tag{D.4}$$

Additionally, Δt can be expressed as a function of the absolute velocity and the angle of departure as well. Here, it is assumed that both z_b^o and z_b^i are zero. This gives the equation

$$\|\mathbf{v_b^o}\| \sin(\gamma)\Delta t - \frac{1}{2}g(\Delta t)^2 = 0, \tag{D.5}$$

and solving this for Δt results in

$$\Delta t = \frac{2\|\mathbf{v_b^o}\| \sin(\gamma)}{g}. \tag{D.6}$$

By substitution of Equation (D.6) into Equation (D.4), the horizontal distance can be expressed as a function of $\mathbf{v_b^o}$ and γ, by

$$x_b^i = x_b^o + \frac{2\|\mathbf{v_b^o}\|^2}{g} \sin(\gamma)\cos(\gamma). \tag{D.7}$$

Using the trigonometric relation

$$\sin(2\gamma) = 2\sin(\gamma)\cos(\gamma), \tag{D.8}$$

this relation can be simplified to

$$x_b^i = x_b^o + \frac{\|\mathbf{v_b^o}\|^2 \sin(2\gamma)}{g}. \tag{D.9}$$

Similarly, the vertical distance can be expressed as a function of $\mathbf{v_b^o}$ and γ as well. Substitution of Equation (D.6) into Equation (D.2) gives the maximum height as

$$z_b^m = z_b^o + \frac{\|\mathbf{v_b^o}\|^2 \sin^2(\gamma)}{2g}. \tag{D.10}$$

For brevity, the following notation will be used from here on

$$\Delta x = x_b^i - x_b^o, \tag{D.11}$$
$$\Delta z = z_b^m - z_b^o. \tag{D.12}$$

This simplifies Equation (D.9) and Equation (D.10) further down to

$$\Delta x = \frac{\|\mathbf{v_b^o}\|^2 \sin(2\gamma)}{g}, \tag{D.13}$$
$$\Delta z = \frac{\|\mathbf{v_b^o}\|^2 \sin^2(\gamma)}{2g}. \tag{D.14}$$

Division of Δz by Δx yields a relation between the angle of departure, the maximum ball height and the distance, namely

$$\frac{\Delta z}{\Delta x} = \frac{\|\mathbf{v_b^o}\|^2 \sin^2(\gamma)}{2g} \cdot \frac{g}{\|\mathbf{v_b^o}\|^2 \sin(2\gamma)}, \tag{D.15}$$
$$\frac{\Delta z}{\Delta x} = \frac{\sin^2(\gamma)}{4\sin(\gamma)\cos(\gamma)}. \tag{D.16}$$

Using

$$\tan(\gamma) = \frac{\sin(\gamma)}{\cos(\gamma)}, \tag{D.17}$$

this can be simplified as

$$\frac{\Delta z}{\Delta x} = \frac{\tan(\gamma)}{4}, \tag{D.18}$$

which is the final form of this relation.

Appendix E

Derivation of the reference angle for the platform

The platform makes an angle θ with the horizontal. The ball impacts the platform with an angle of incidence β and leaves the platform with an angle of departure γ. The angle of incidence and the reference angle of departure are known, from which the reference angle of the platform can be derived. See Figure E.1 for a sketch of the platform, ball velocities and all relevant angles. It is assumed that the angle $\angle A$ of the ball velocities with respect to the platform normal are equal for both the incoming and outgoing instances, indicated with the dots.

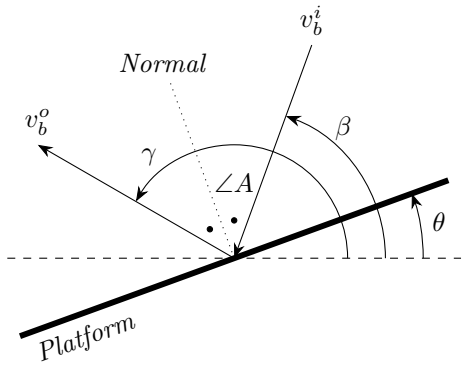

Figure E.1: Visualisation of the impact of the ball on the platform and the involved angles.

From Figure E.1, it can be seen that

$$\gamma - \beta = 2\angle A \tag{E.1}$$

and that

$$\gamma - (\theta + \frac{1}{2}\pi) = \angle A. \tag{E.2}$$

Substitution of Equation (E.2) into Equation (E.1), gives

$$\gamma - \beta = 2\gamma - 2\theta - \pi. \tag{E.3}$$

Rewriting this for θ results in

$$\theta = \frac{\gamma + \beta - \pi}{2}. \tag{E.4}$$

Appendix F

Calculation of platform trajectory 2D bouncing

The platform starts at time t_1 with an angle of $\theta_1 = 0$. The ball is expected to impact the platform at time t_i and the interval over which a constant angle is required, is taken as 2σ. This results in values for t_3 and t_4 are therefore the same as those calculated in Equation (B.1) and Equation (B.2). Since this profile is symmetrical around t_i, only the calculation of the trajectory from t_1 to t_3 is shown. The part between t_4 and t_6 can be obtained by mirroring and negating the first part of the trajectory.

To obtain the reference angle with maximum acceleration and deceleration, two second-order polynomials are used: one between t_1 and t_2, the other between t_2 and t_3. The values for t_1 and t_2 are found from the relation between the maximum velocity, which occurs at t_2, and the maximum acceleration.

The maximum angular velocity can be expressed as

$$\omega_{max} = \frac{2\theta_{ref}}{t_3 - t_1} \tag{F.1}$$

and as

$$\omega_{max} = \frac{1}{2}\alpha_{max}(t_3 - t_1), \tag{F.2}$$

t_1 can be found as

$$t_1 = t_3 - 2\sqrt{\frac{\theta_{ref}}{\alpha_{max}}}. \tag{F.3}$$

Since t_2 is exactly between t_1 and t_3, this is

$$t_2 = t_3 - \sqrt{\frac{\theta_{ref}}{\alpha_{max}}}. \tag{F.4}$$

The angle θ_2 at time t_2 can now be found using

$$\theta_2 = \frac{1}{2}\omega_{max}(t_2 - t_1). \tag{F.5}$$

Between t_1 and t_2, a second order polynomial

$$\theta(t) = a_1 t^2 + a_2 t + a_3 \tag{F.6}$$

is used, with boundary conditions

$$\theta(t_1) = 0 \tag{F.7}$$
$$\theta(t_2) = \theta_2 \tag{F.8}$$
$$\omega(t_2) = \omega_{max}. \tag{F.9}$$

This results in the coefficients

$$\begin{bmatrix} a_1 \\ a_2 \\ a_3 \end{bmatrix} = \frac{1}{(t_1 - t_2)^2} \begin{bmatrix} -(\theta_2 + \omega_{max} t_1 - \omega_{max} t_2) \\ (\omega_{max} t_1^2 - \omega_{max} t_2^2 + 2\theta_2 t_2) \\ (t_1(t_1\theta_2 - 2t_2\theta_2 + \omega_{max} t_2^2 - \omega_{max} t_1 t_2)) \end{bmatrix}. \tag{F.10}$$

Between t_2 and t_3, a second order polynomial

$$\theta(t) = b_1 t^2 + b_2 t + b_3 \tag{F.11}$$

is used, with boundary conditions

$$\theta(t_2) = \theta_2 \tag{F.12}$$
$$\omega(t_2) = \omega_{max} \tag{F.13}$$
$$\theta(t_3) = \theta_{ref}. \tag{F.14}$$

This results in the coefficients

$$\begin{bmatrix} b_1 \\ b_2 \\ b_3 \end{bmatrix} = \frac{1}{(t_2 - t_3)^2} \begin{bmatrix} (\theta_{ref} - \theta_2 + \omega_{max} t_2 - \omega_{max} t_3) \\ -(2t_2\theta_{ref} - 2t_2\theta_2 + \omega_{max} t_2^2 - \omega_{max} t_3^2) \\ (\omega_{max} t_2^2 t_3 + \theta_{ref} t_2^2 - \omega_{max} t_2 t_3^2 - 2\theta_2 t_2 t_3 + \theta_2 t_3^2) \end{bmatrix}. \tag{F.15}$$

Appendix G

Simulation model 2D bouncing

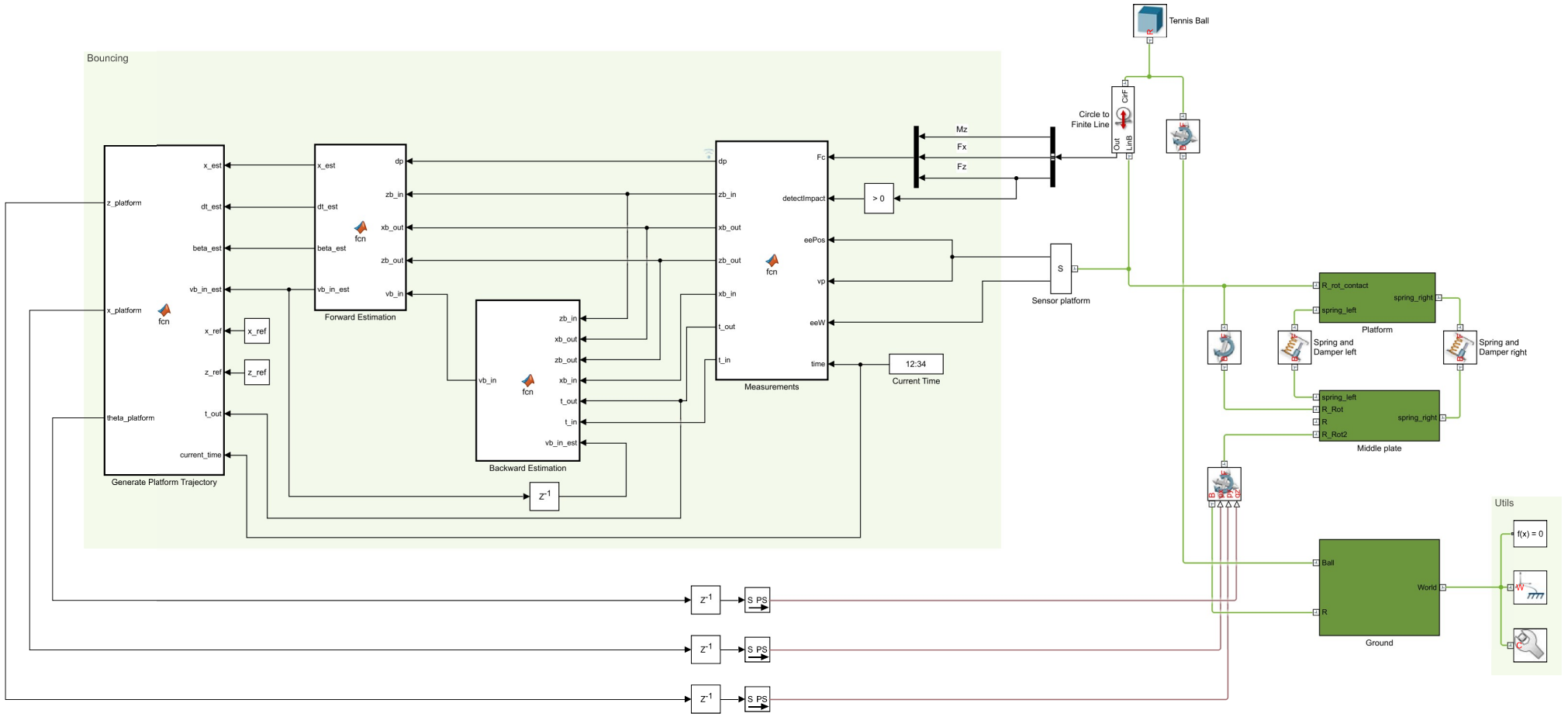
Bouncing
x_est
dt_est
beta_est
vb_in_est
x_ref
z_ref
t_out
current_time
z_platform
x_platform
theta_platform
fcn
Generate Platform Trajectory
x_ref
z_ref
dp
zb_in
xb_out
zb_out
vb_in
Forward Estimation
zb_in
xb_out
zb_out
xb_in
t_out
t_in
vb_in_est
vb_in
fcn
Backward Estimation
Z-1
dp
zb_in
xb_out
zb_out
xb_in
t_out
t_in
fcn
Fc
detectImpact
eePos
vp
eeW
time
Measurements
Mz
Fx
Fz
> 0
12:34
Current Time
S
Sensor platform
Tennis Ball
Circle to Finite Line
Out
Ball
R_rot_contact
spring_right
spring_left
Platform
Spring and Damper left
Spring and Damper right
R_Rot
R
R_Rot2
Middle plate
World
Ground
Utils
f(x) = 0
S PS

Appendix H

Plagiarism Report